YIPEEO: Yield Prediction and Estimation using Earth Observation

[Impact Assessment Report v2.0]

[IAR]

Version 2.0

[21/02/2025]

Submitted by:

TU Wien – Department of Geodesy and Geoinformation

in cooperation with:

CzechGlobe and EODC

This document was compiled in response of the ESA/AO/1-11144/22/I-EF: ESA Express Procurement Plus – EXPRO+ Theme 2 - Yield Estimation & Forecasting.

This document provides the Impact Assessment Report (IAR) which consists of the Science Chapter (D5.1) and the Societal Impact Chapter (D6.1) of the project YIPEEO.

Number of pages: 61

Authors:	Felix Reuß (FR), Emanuel Büechi (EB), Wouter Dorigo (WD), Maud Formanek (MF), Lenka Bartošová (LB), Miroslav Pikl (MP)		
Circulation (internal):	Project consortium		
External:	ESA		
Issue	Date	Details	Editor
0.1	31.8.2024	First draft	FR
1.0	31.8.2024	To ESA	FR
2.0	12.1.2025	Update Societal impact chapter	LB

For any clarifications please contact Felix Reuß (felix.reuss@geo.tuwien.ac.at).

Table of Contents

Executive Summary

This document constitutes the first version of the Impact Assessment Report as a result of Task 5, as described in the proposal of the ESA YIPEEO project.

1. Science

.1.1 Assess impact of the 2018 drought on yield on different crop types in north-western Europe using the Experimental dataset and upscaled yield data

Due to the unforeseen long-term sick leave of Mariette Vreugdenhil we can't present updates on her paper for Science case 1. We will provide an update on this as soon as possible. In the following we present therefore only the second paper related to the Science Case 1 focusing on the value of different soil moisture products for yield prediction.

.1.1.1 Introduction

Yield prediction is crucial for optimizing agricultural practices by enabling precise resource allocation and maximizing crop productivity. Accurate yield predictions also help mitigate financial risks for farmers by informing decisions on crop selection and market timing. Furthermore, they contribute to environmental sustainability by promoting efficient use of inputs such as water, fertilizers, and pesticides. In drought years, harvest forecasts are essential for the early detection of a lack of food supply. This allows countermeasures such as artificial irrigation or importing food. A key indicator for drought conditions is Surface Soil Moisture (SSM). It is sensitive to weather and climate patterns and to precipitation and temperature dynamics. Since soil moisture is an important variable that influences plant growth and thus crop yield, it was used in numerous studies for yield prediction, mostly as an input to machine learning models. Bushong et al. (2016) found that including satellite derived soil moisture in the prediction of grain yield led to an increase in R2 of 0.09. Moreover, White et al. (2020) assessed the value of SMOS SSM for canola yield prediction and observed an improved accuracy in the majority of the tested ecodistricts. In another study, Buecchi et al. (2023) used in their study CCI SSM and SWI for the prediction of wheat and maize yield and found that especially in drought years, SSM is one of the most important predictors. Chen et al. (2014) demonstrated in their study the potential of SSM to quantify the water driven variability in NDVI. Amor et al. (2013) used AMSR-E soil moisture and LAI data for maize yield prediction and concluded that AMSR-E soil moisture tends to be more biased under the presence of high vegetation and suggested updating rootzone soil moisture by near-surface soil moisture assimilation. Finally, Potopova et al. (2020) compared ASCAT SWI for top soil and root zone to model yield losses in Moldova for three crop types and observed a higher correlation for top soil moisture product with yield. While these studies demonstrated the general value of soil moisture products for yield prediction, an in-depth assessment of its potentials and limitations has not yet been carried out. In this science case we will compare a satellite derived and a model soil moisture product for the prediction of spring barley yield in Austria, Czech Republic (both NUTS4 level) and Germany (NUTS-3 level) for the years 2016-2022. In detail, the science case will focus on the following research issues: How much of the spring barley yield variability can be explained only by soil moisture? How does yield prediction based on satellite derived soil moisture compare to yield prediction based on modelled soil moisture? How transferable are the yield prediction models over space and over time?

.1.1.2 Materials

The studies uses the HSAF Soil Moisture Product (Hydrology Satellite Application Facility Soil Moisture Product). This product is developed under the EUMETSAT's (European Organisation for the Exploitation of Meteorological Satellites) H-SAF program and uses C-band microwave satellite observations from the ASCAT (Advanced Scatterometer) satellite mission to estimate the water content in the top few centimeters of soil (H SAF, 2021). In this study SSM version H119 and H120 at a 12.5km sampling are used. In addition, we used the Volumetric Soil Water Layer 1 (SWVL1) variable from the ERA5 reanalysis dataset that represents the volumetric soil moisture content in the topmost soil layer, ranging from 0 to 7 cm depth. This variable quantifies the amount of water contained within the soil matrix in the specified layer, expressed as a fraction of the total soil volume. It is provided on 0.25°x0.25° grid in a temporal resolution of 1 hour (European Centre for Medium-Range Weather Forecasts, 2017).

For all NUTS regions, the grid points closest to the centroid of the NUTS region was selected from the two SSM datasets. Subsequently, time series for the period April to the end of June were extracted to cover the vegetation period of Spring barley up to one month before harvest. Afterwards, the time series were resampled to 14 daily time steps. This time window was selected as compromise to capture soil moisture variations over time but to avoid a too high number of input features for the machine learning model. For the 14 daily time steps, the statistics min, max, and mean were calculated and used as input features for the model.

As a model we used a Feed Forward Neural Network with 2,500 hidden nodes and dropout as a regularization mechanism to prevent overfitting. Subsequently, we trained individual Feed Forward Neural Networks for the soil moisture products using the absolute spring barley yield as a target variable. After the prediction, we calculated the error metrics RMSE, MAE, and MAPE for the test data.

.1.1.3 Results:

In a first step, we assessed the predictive power of the two soil moisture products for spring barley yield. For this we used the same random train/test split over all countries and years for both soil moisture products. Tab. 1 outlines the error metrics for both products. The HSAF based model achieved a R^2 of 0.23, a RMSE of 0.90 and a MAE of 0.69. The HSAF SSM product can thus explain 23% of the variability of spring barley yield in the data set. The values for the ERA5 model are better for most metrics. The model achieved a R2 of 0.36, RMSE 0.84 and MAE 0.66. The ERA5 SWVL1 product can thus explain 36% of the variability of spring barley yield in the data.

Table 1: Error metrics for the HSAF SSM product and the ERA5 SWVL1 using a random train/test split.

R^2	RMSE	MAE	MAPE	R^2	RMSE	MAE	MAPE
0.23	0.90	0.69	0.15	0.36	0.84	0.66	0.14

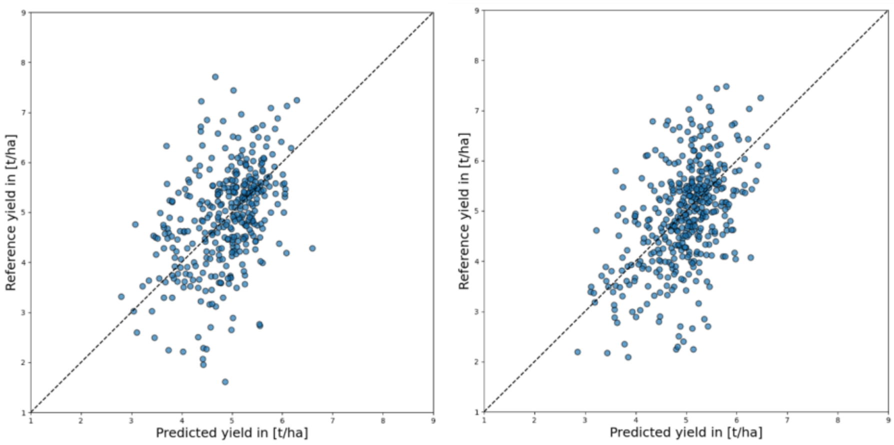

Figure 1: Correlation plots between the predicted and reference yield for the HSAF soil moisture product (left) and the ERA5 product (right).

Fig. 1 illustrates the correlation plots between the predicted and reference yield for both products. Since the points are distributed along the diagonal and are not just randomly distributed or centered around the mean value, the model is able to extract patterns from the soil moisture data that enable an estimation of the yield. However, low reference yields show the tendency to be overestimated for both input products. Overestimations occur to at a similar frequency for both products but more extreme cases can be found for the HSAF product.

Table 2: Error metrics for the HSAF SSM product and the ERA5 SWVL1 when training a model in two countries and testing it in the remaining country.

	R^2	RMSE	MAE	MAPE	R^2	RMSE	MAE	MAPE
AT	0.26	0.94	0.72	0.15	0.27	0.92	0.74	0.16
CZ	0.28	0.90	0.70	0.15	0.36	0.83	0.64	0.13
DE	0.27	0.90	0.70	0.14	0.31	0.86	0.68	0.14

Subsequently, we tested the spatial and temporal transferability of the models. This way it is possible to make a statement about the robustness of SSM as a predictor. First, we conducted a leave one out cross validation on country level. We subsequently trained a model on the data of two of the three countries and tested it on the data of the remaining country. Tab. 2 outlines the achieved error metrics for both products and the three countries. As can be seen from the table, the achieved metrics are comparable to those of the random split over space and time for both products. The metrics for Austria are the worst, whereby the decline here is higher for the ERA5 SWVL1 with 0.08 for RMSE and MAE than for HSAF (0.4 for RMSE 0.3 for MAE).

Okomentoval(a): [BP1]: ED: are these metrics acceptable, to be concluded as useful?

Okomentoval(a): [RF2R1]: We rephrased the first research issue in this science case to make the goal clearer: How much of the spring barley yield variability can be explained solely by soil moisture. We added here now the R² value for the two products to answer this question. In the paper based on this science case we will also focus on this aspect and make the general idea clearer (not proposing yield prediction only on soil moisture but assessing how much of the yield can be explained by soil moisture)

Fig. 2 illustrates correlations plots for the two products and all countries. The correlation plots show a similar distribution as for the random train test split. Here, too, there is a significant overestimation of low crop yields. This is particularly noticeable in Austria. Overall, both soil moisture products again show very similar results.

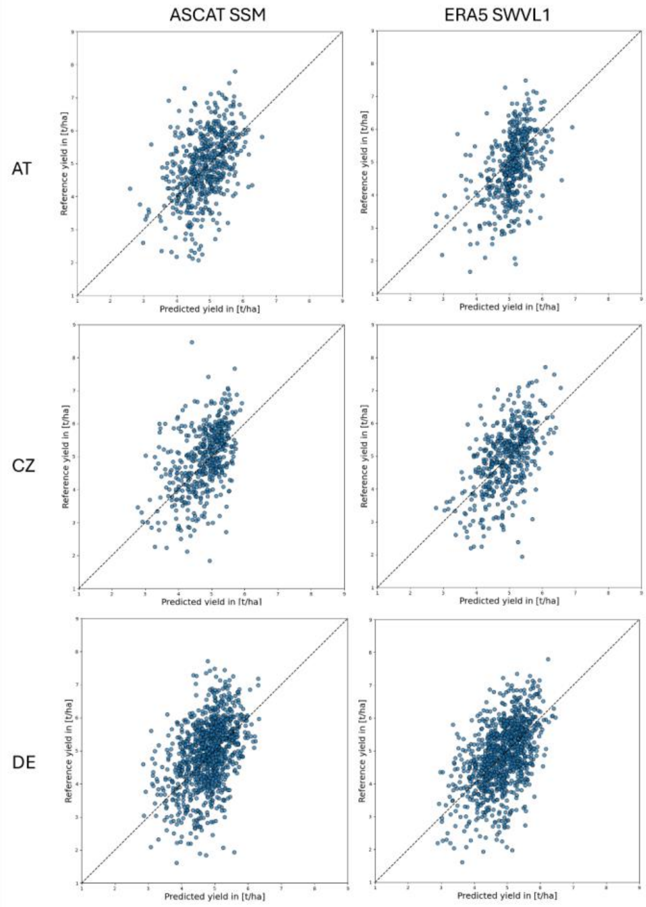

Figure 2: Correlation plots between the predicted and reference yield for the HSAF soil moisture product (left) and the ERA5 product (right) for Austria (AT), Czech Republic (CZ) and Germany (DE).

Afterwards, we tested the temporal transferability. Here, we performed a leave

one year out cross validation. Thus, the model was subsequently trained on the data of all years except for one and then tested for the left-out year.

Tab. 3 illustrates the results for the temporal leave-out experiment. The accuracies achieved differ significantly between the years. For the years 2021, 2016 and 2019, metrics for both products are only up to 0.1 worse than the RMSE and the MAE in a random train/test split. In 2017, 2018 and 2022, the error values are already significantly larger. By far the greatest deterioration can be observed for 2020. For this year, the deviation is higher for ERA5 (RMSE increases by 0.76) compared to HSAF (RMSE increases by 0.63). The analysis thus shows that temporal transferability is more difficult than spatial transferability. For a temporal transfer, good results were only achieved for a few years.

Table 3: Error metrics for the HSAF SSM product and the ERA5 SWVL1 when training a model in all but one year and testing it in the left-out year.

	HSAF SSM			ERA5 SWVL1		
	RMSE	MAE	MAPE	RMSE	MAE	MAPE
2016	1.01	0.84	0.18	1.02	0.80	0.18
2017	1.12	0.91	0.20	1.17	0.94	0.20
2018	1.28	1.01	0.20	1.52	1.20	0.23
2019	1.07	0.82	0.18	1.23	1.02	0.22
2020	1.53	1.23	0.30	1.60	1.32	0.34
2021	1.01	0.78	0.16	0.97	0.76	0.15
2022	1.13	0.91	0.20	1.28	1.02	0.19

The significant differences in the temporal transferability can be partly explained by the differences in the correlation between the mean SSM and the yield at the end of the season. The correlation heatmaps in Fig. 3 show the yearly correlation between the mean SSM of different calendar weeks and the yield at the end of the season for the HSAF and the ERA5 product.

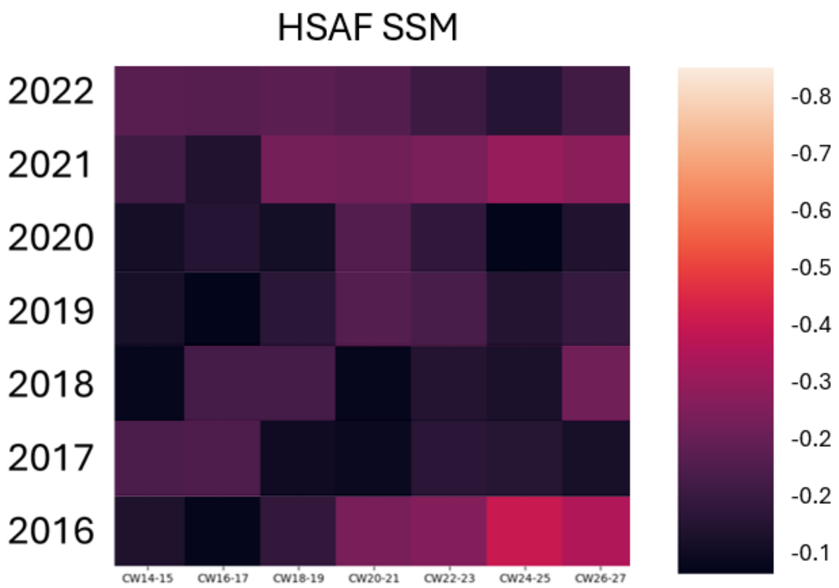

Figure 4: Correlation heatmaps between the mean soil moisture at different calendar weeks and yield at the end of the seasons for the years 2016-2022 for the HSAF product.

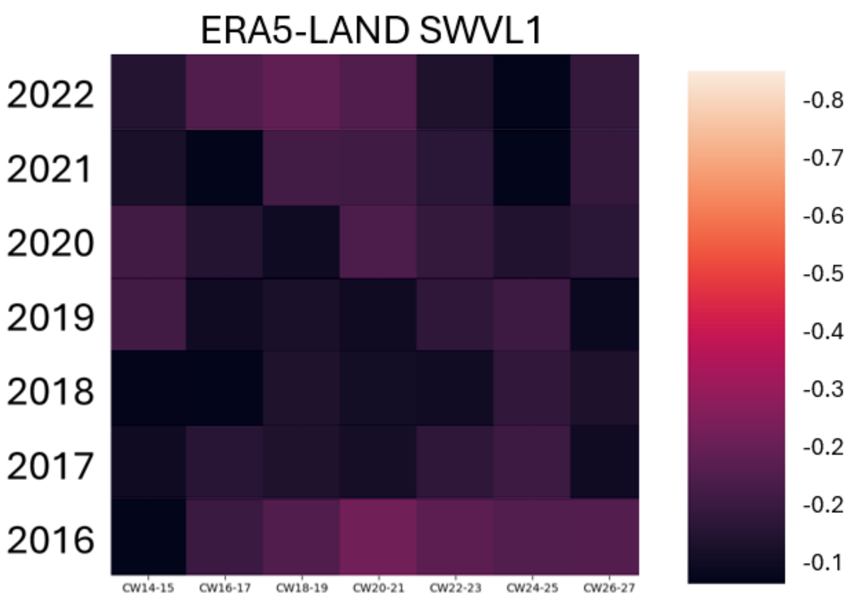

Figure 3: Same as figure 3 but for the ERA5 SWVL1 product.

As can be seen from the figure, the differences in the correlation coefficients are significant between the years. For both products, the coefficient is highest for the year 2016, which is one of the years with the best error metrics. Low coefficients occur in 2017, 2018 and 2020, where the values for the HSAF product are slightly higher than for the ERA5 product. If we look at the values for the respective calendar weeks, we can see strong differences between the years. For HSAF, the highest values in 2016 and 2021 are in weeks 24-25 (mid-June). In 2017, 2018 and 2022, on the other hand, the higher correlations occur in the early calendar weeks (period April to early May). The correlation values for ERA5 are slightly lower overall.

Okomentoval(a): [BP3]: ED: can we conclude which products are being more useful for yield prediction?

Okomentoval(a): [RF4R3]: We didn't not want to draw a conclusion only from this plot. In our paper based on this science case we will provide a clear picture in which regions one product performs better and if one product is overall better for spring barley yield prediction in Central Europe. Our current analysis suggest that the ERA5 product shows better performance in the alpine region and Eastern Germany and show overall slightly better accuracy.

.1.1.4 Outlook

In a next step, we aim to understand the performances differences between the years in more detail. In particular, we will investigate if soil moisture variations or yield variations are in those years the main driver for the decline of the model performance. This will help us understand under which conditions soil moisture has a higher predictive power and under which a lower performance can be expected. Moreover, we will test the accuracies for predictions with a lead time longer than one month. Finally, we will also replace the current ASCAT SSM product with the newest release which includes landcover trend correction and should capture drought conditions better.

Bibliography

Bushong, J.T., Mullock, J.L., Miller, E.C., Raun, W.R., Klatt, A.R. and Arnall, D.B. (2016). Development of an in-season estimate of yield potential utilizing optical crop sensors and soil moisture data for winter wheat. *Precision Agriculture*, 17(4), pp.451–469. doi:https://doi.org/10.1007/s11119-016-9430-4.

Bueechi, E., Fischer, M., Crocetti, L., Trnka, M., Grlj, A., Zappa, L. and Dorigo, W. (2023). Crop yield anomaly forecasting in the Pannonian basin using gradient boosting and its performance in years of severe drought. *Agricultural and Forest Meteorology*, [online] 340, p.109596. doi:https://doi.org/10.1016/j.agrformet.2023.109596.

Chen, T., de Jeu, R.A.M., Liu, Y.Y., van der Werf, G.R. and Dolman, A.J. (2014). Using satellite based soil moisture to quantify the water driven variability in NDVI: A case study over mainland Australia. *Remote Sensing of Environment*, 140, pp.330–338. doi:https://doi.org/10.1016/j.rse.2013.08.022.

European Centre for Medium-Range Weather Forecasts (2017). "ERA5 Reanalysis." Copernicus Climate Change Service (C3S) Climate Data Store (CDS). https://doi.org/10.24381/cds.adbb2d47

H SAF (2021): ASCAT Surface Soil Moisture Climate Data Record v7 12.5 km sampling - Metop, EUMETSAT SAF on Support to Operational Hydrology and Water Management, DOI: 10.15770/EUM_SAF_H_0009. http://doi.org/10.15770/EUM_SAF_H_0009

Ines, A.V.M., Das, N.N., Hansen, J.W. and Njoku, E.G. (2013). Assimilation of remotely sensed soil moisture and vegetation with a crop simulation model for maize yield prediction. *Remote Sensing of Environment*, 138, pp.149–164. doi:https://doi.org/10.1016/j.rse.2013.07.018.

Potopová, V., Trnka, M., Hamouz, P., Soukup, J. and Castraveț, T. (2020). Statistical modelling of drought-related yield losses using soil moisture-vegetation remote sensing and multiscalar indices in the south-eastern Europe. *Agricultural Water Management*, [online] 236, p.106168. doi:https://doi.org/10.1016/j.agwat.2020.106168.

White, J., Berg, A.A., Champagne, C., Zhang, Y., Aston Chipanshi and Bahram Daneshfar (2020). Improving crop yield forecasts with satellite-based soil moisture estimates: An example for township level canola yield forecasts over the Canadian Prairies. *International Journal of Applied Earth Observation and Geoinformation*, 89, pp.102092–102092. doi:https://doi.org/10.1016/j.jag.2020.102092.

.1.2 Assessment of the impact of the war in Ukraine on production of main crops

.1.2.1 Introduction

In SC-2 we assess the impact of the war in Ukraine, which started in February 2022, on the crop yields for that year. In the proposal, we suggested investigating the change in predicted and harvested yields based on early season predictions as developed in Task 3 and available in the experimental dataset (ED). Based on the results of the ED, an investigation of the early-season predictions may not be that useful due to their rather low performance. Instead, we developed a new approach to assess the impact of the war on crop yield losses. In our database, we have some data from Ukraine on field level. Since this is mainly in the west of Ukraine and from the year before 2022, it is not that much suited for this task. The regional data that we have from Ukraine is better suited since it is available from 2017 to 2022. Hence, the first year of the Russian invasion of Ukraine is covered. In addition, we have an extensive database of regional crop yield data from central Europe (Fig. 5). The results of the ATBD have shown that directly transferring the crop yield forecasts trained in central Europe does not work well in forecasting crop yields in Ukraine. This may be explained by the different climate classes (C: warm temperate in central Europe and D: snow for Ukraine cf. Fig. 5). Hence, we suggest using transfer learning to improve the forecasts of Ukraine. Using this method is more promising to achieve reasonable results that can be used to assess the impacts of the war in Ukraine on their crop production. Our forecasts for 2022 are then compared to the observed values to see how much of the crop yields can be explained by weather. The question we aim to answer is if there are variabilities in the crop yields not explainable by the weather and additional uncertainties. In addition, it will be an interesting case study to test transfer learning for crop yield forecasting in different climatic zones. There is only one study known to us that has done so (Wang et al., 2018)

.1.2.2 Methods

For the regional scale crop yield forecasts we have data available for central Europe for the years 2000-2022 and for Ukraine from 2017-2022. The climate zones are different between these two regions (Cfb in central Europe and Dfb in Ukraine cf. Fig. 5). Hence, for setting up a crop yield forecasting model based on machine learning the transferability has to be checked carefully. Simply training the model with data from all regions may not work out. Hence, we tried different approaches to optimize the crop yield forecasts for Ukraine:

1) Using leave-one-**country**-out cross-validation to check how well a model can forecast countries from which it has not seen data.
2) Using leave-one-**year**-out cross-validation and using the data from Ukraine for transfer-learning. I.e. the model is trained using all data from central Europe and all years except for one year. The model is then retrained with data from Ukraine except for the testing year. Finally, the model is tested on the Ukraine data of the testing year.

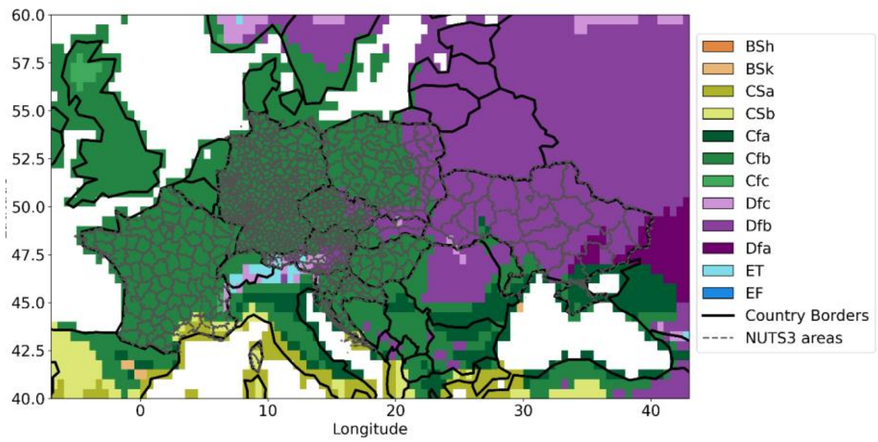

Figure 5: Overview of the study area, the used NUTS3 regions and their climate classes according to Köppen-Geiger (Kottek et al., 2006)

The model run is only done for a lead time of 1 week before the harvest. With this, we can ensure that the model obtains all climatic information throughout the growing season. Since the goal is to explain crop yield losses in Ukraine by war or climatic conditions, there is not much use in running the model in forecasting mode with lead times longer than this. As predictors, we only use ERA5-Land data due to its availability for the whole time-series where we have crop yield data. Also, it provides all kinds of climatological information that can be used to successfully train our model (temperature, precipitation, soil moisture, potential evapotranspiration, actual evaporation, and net surface radiation). Since we do not have crop classification maps of Ukraine, S1 and S2 data was not possible to extract on this scale. Also, we do not want to include vegetation information in the model to strictly only model it by climatic conditions. The data is extracted as mean observations per region and day. This data is then resampled to monthly means starting 4 months before the harvest. For the harvest dates, we use the information from the crop calendar of the joint research centre for the central European data (JRC, 2024) and from the US Department of Agriculture (USDA, 2024) for Ukraine. We are doing the modelling for the three crops maize, winter wheat and spring barley. For validation we use Pearson's correlation between observed and forecasted crop yields as well as normalized Root Mean Square Error (nRMSE), which is the RMSE normalized by the mean observed crop yields.

.1.2.3 Results

Initial results without transfer learning showed poor performance for the leave-one-country-out cross-validation (Fig. 6). The correlations between forecasted and observed crop yields are below 0.5 for all countries and crops except for winter wheat in France and the nRMSE are high. The impact of the climate zones does not seem to be big, since all countries have a low performance. Still, Ukraine has among the lowest correlations for maize and winter wheat and average for spring barley. There is much room for improvement which we explore in the next step with transfer learning.

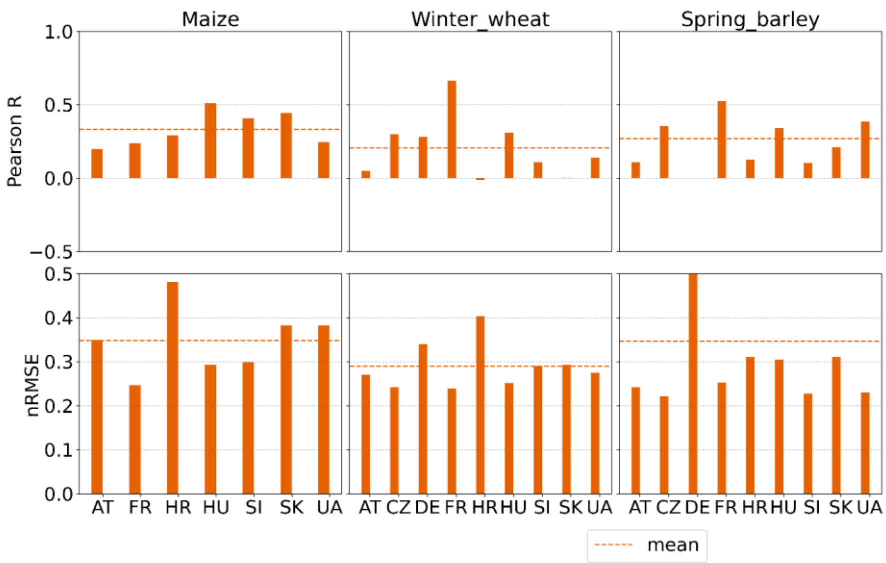

Figure 6: Results of the leave-one-year-out cross-validation for the three crops without transfer-learning

Transfer learning significantly improved the forecasts (Fig. 7). The leave-one-year-out cross-validation revealed that the model could effectively predict crop yields in Ukraine for the 3 crops.

The maize model achieved correlations of around 0.7 with rather high errors (of around 30%), though. The spring barley and winter wheat models had much lower errors (around 15%) and high correlations for barley (~0.7) and medium correlations for wheat (~0.5). The results are much better in almost all cases using transfer learning compared to the initial model. The year 2022, after the start of the war, has very good results compared to the other years. This indicates the crop yields can largely be explained by the climatic conditions even in that year. However, it is crucial to note that our model used average crop yields per region. We do not have any data about the total yields per area nor about how much area was cultivated. This doesn't fully capture the complex realities on the ground in 2022:

- Many farmers in invaded areas were unable to start crop cultivation due to the conflict.
- Farmers who did cultivate crops often had limited resources and faced high uncertainties about whether they could safely harvest.
- Fields that were successfully harvested by the end of 2022 may have shown normal crop growth patterns.
- The total cultivated area in affected regions was significantly reduced compared to previous years.

Having mentioned this limitation, we further analysed the results to see if the regions in the southeast, occupied by Russia, are specifically affected by low crop yields. Fig. 8 shows the forecasted and observed crop yields in 2022 for all regions in Ukraine. It shows that particularly the occupied regions in the southeast have very low observed and forecasted crop yields. Hence, we can again state that the low crop yields in this area can be explained by the unfavourable weather conditions. The regions that were regained by Ukraine (but were still occupied in 2022) showed rather higher crop yields than expected for winter wheat and spring barley.

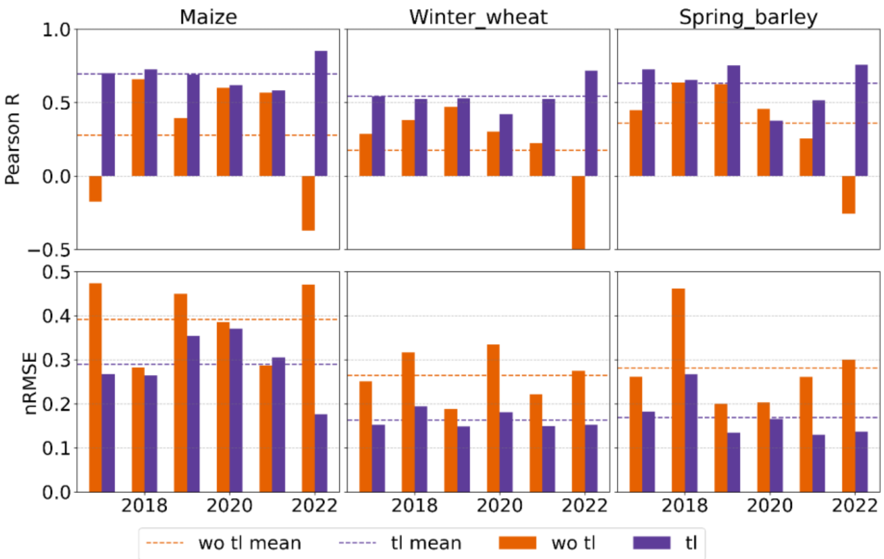

Figure 7: Results of the leave-one-year-out cross-validation for Ukraine, with (purple) and without (orange) transfer learning.

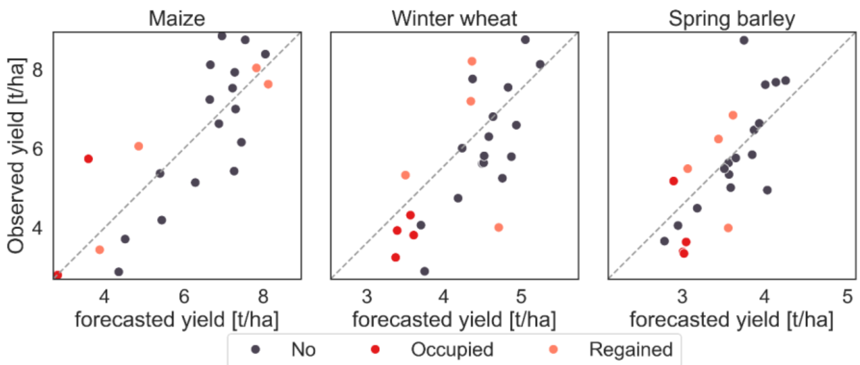

Figure 8: results of the crop yield forecasts in 2022 showing all regions of Ukraine: red are the areas in the southeast that are completely occupied by the Russians (i.e. Donetsk, Zaporizhzhya, Luhansk, and Kherson) - orange are the regions that have been occupied for some time by the Russians but were regained be Ukraine (i.e., Mykolayiv, Sumy, Kharkiv, Chernihiv, and Kyivska - for the latter we have no crop yield data). Estimations for that are based on the Ukraine war map provided by crisisgroup.org

Okomentoval(a): [BP5]: ED: I had also a comment to this x-axis is this metric t/ha or dt tons/ha?

Okomentoval(a): [BPE6R5]: Yes, these are as well t/ha

As a last analysis, we looked at the four occupied regions in more detail. We evaluated how well the model captures the annual variabilities of the crop yields over the years 2017-2022 (Fig. 9). This showed that the maize forecasts are quite bad. For the other two crops the forecasts are better. The results show again that the low crop yields in 2022 are not exceptional and were to be expected by the climatic conditions.

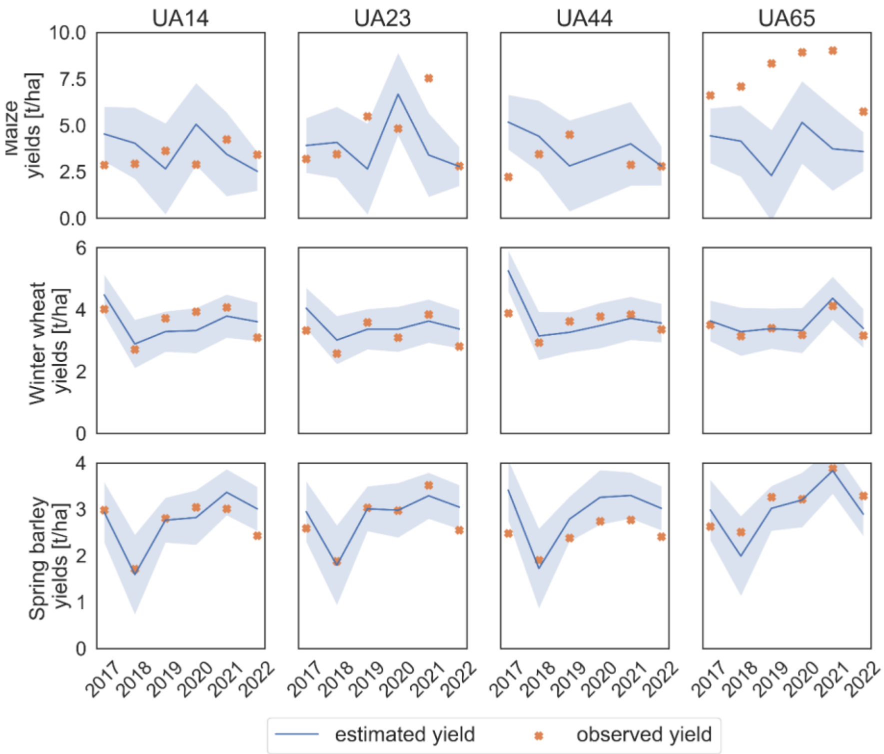

Figure 8: Results of the leave-one-year-out cross-validation for the 4 regions occupied by Russia: UA14 - Donetsk, UA23 - Zaporizhzhya, UA44 - Luhansk, UA65 - Kherson. The error bands are based on the RMSE of the models per year.

.1.2.4 Conclusion:

The results show that transfer learning is a powerful tool for crop yield forecasting in a country where we do not have much data. The model can even be applied in different climatic conditions. By doing so, we have implemented a crop yield forecasting system for Ukraine and evaluated its performance with a focus on the year 2022, i.e. after the Russian invasion. The results showed that crop yields in the occupied regions were low in 2022 compared to other areas. This is not exceptional, though, as these regions always have rather low average crop yields. The low crop yields can mainly be explained by the unfavourable meteorological conditions. However, we also pointed out that the analysis has some flaws, as the average crop yields in the region do not well reflect the actual impacts the war has. Instead, we could only show that the farmers who were still able to cultivate crops achieved average crop yields considering the meteorological conditions.

As a next step we will further elaborate on the results presented here and write a paper about spatial transfer learning for crop yield forecasting with the results shown here as a case study for applicability of such methods. Also, we are still in contact with Svitlana Kokhan, who provided us with the crop yield data from Ukraine. She may provide us with more crop masks or total yields per area which we will use to improve the results and take the actual impacts of war further into account.

Okomentoval(a): [BP7]: ED: we should as well investigate the possibility to compare these results with the data provided by VISTA. They presented their results on EO4Agric Workshop: Resilience under Extreme Circumstances – Harvest and Yield Estimation for Ukraine 2023.

Okomentoval(a): [BPE8R7]: This would be very interesting indeed. The last update I got from Espen was that they will not be able to share the data, right? However, if anything changes, we would still like to do this comparison

Bibliography

JRC (accessed in 2024). Crop Calendar. https://agri4cast.jrc.ec.europa.eu/dataportal/

Kottek, M., J. Grieser, C. Beck, B. Rudolf, and F. Rubel, 2006: World Map of the Köppen-Geiger climate classification updated. *Meteorol. Z.*, **15**, 259-263. DOI: 10.1127/0941-2948/2006/0130.

USDA (accessed in 2024). Foreign agriculture service – crop calendars for Ukraine, Moldova, and Belarus. https://ipad.fas.usda.gov/rssiws/al/crop_calendar/umb.aspx

Wang, A. X., Tran, C., Desai, N., Lobell, D., and Ermon, S. (2018). Deep transfer learning for crop yield prediction with remote sensing data. In Proceedings of the 1st ACM SIGCAS Conference on Computing and Sustainable Societies, COMPASS 2018, volume 18. Association for Computing Machinery, Inc

.1.3 Assessing the value of irrigation for enhancing crop production and mitigating yield losses

Irrigation is the largest contributor of freshwater consumption globally, in many instances leading to negative environmental effects. However, irrigated agriculture can play an important role in ensuring food security by increasing crop yields. Sustainable irrigation practices aim therefore at maximizing crop production, while reducing the negative impact of extensive irrigation. Indeed, both the correct timing of irrigation, i.e., when the vegetation most needs it, as well as the amount of water allocated to the field are key elements to guarantee the highest water use efficiency.
Recently, satellite soil moisture products have been used to derive timing and amounts of water used for irrigation on a quasi-field scale (Zappa et al., 2021). Combining this information with water balance models (e.g., SoilClim (Hlavinka et al., 2011; Řehoř et al., 2021)) and crop yield forecasting models can provide insights on the overall contribution of irrigation to the final yield. In this SC, we will first explore how the actual (EO-derived) irrigation impacts the productivity at the end of the season, and then we will investigate how different timings and water volumes could have further improved the crop yields. This study will seek a close interaction with the IRRIGATION+ and 4D-MED activities sponsored by ESA.

In this science case, the impact of irrigation on crop yields is evaluated for a field level dataset comprised of 8092 records located in the Madrid and Lleida regions of Spain (Madrid: 1914 records, Lleida: 6178). The dataset covers the period of 2016 to 2022 and contains yearly records of each field's shape, location and area, the cultivated crop and whether it is irrigated or not. The vast majority of fields are cultivated with either winter barley (45.4%), winter wheat (26.9%) or maize (18.2%). This data alone is sufficient to give a first indication of the importance of irrigation for enhancing crop yield in these regions. Fig. 1 clearly shows that irrigated fields have a much higher yield on average (5.1 ± 1.5 compared to 2.9 ± 1.4 t/ha for winter barley and 5.7 ± 1.6 compared to 3.3 ± 1.5 t/ha for winter wheat). Note that for maize, not enough fields are non-irrigated for results to be statistically significant.

As a next step, irrigation water timings and amounts are estimated based on Earth Observation data from Sentinel-1 and subsequently related to crop yield. For this part of the science case, we focus on the Lleida region due to (a) greater number of records (3674 irrigated fields) and (b) more readily available satellite and ancillary datasets. The Lleida region forms part of the Ebro basin in northeastern Spain, which is characterised by highly irrigated agriculture, covering roughly 10% of

Okomentoval(a): [BP9]: ED: which products are used for that?

Okomentoval(a): [FM10R9]: this is specified further down, but I added it here as well the total area (Isidoro and Aragüés, 2007) and being responsible for up to 90% of the water consumption in the region (Quiroga et al., 2011).

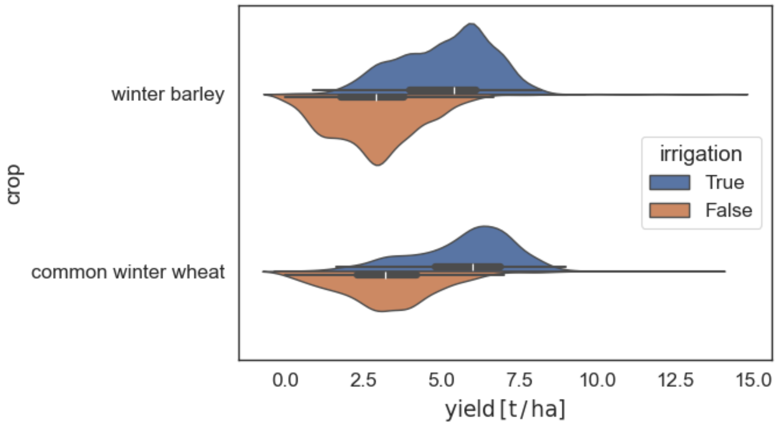

Figure 9: Distribution of crop yields for irrigated and non-irrigated fields, distinguished by crop type.

The irrigation water timings and quantities in the Ebro basin have been derived previously from Earth Observation data for the period 2017-2020 as part of the IRRIGATION+ project using a modified model-independent version of the SM_Delta algorithm (Zappa et al., 2024). This approach detects irrigation events and quantifies the corresponding irrigation amounts by comparing soil moisture from a specific (potentially irrigated) pixel to the average soil moisture found in the surrounding pixels. This approach shows good correlation of irrigation water amounts with reference data for high-resolution soil moisture datasets, for which one can assume that precipitation is constant over several pixel, such that the only difference in soil moisture between neighbouring pixels can be attributed to irrigation (Zappa et al., 2021, Zappa et al., 2024). The SM_Delta approach was applied to the Sentinel-1 surface soil moisture (S1-SSM) product obtained with a first-order radiative transfer model (RT1) (Quast et al., 2023), available at a 500m sampling with 1km resolution.

This dataset from the IRRIGATION+ project could not be used directly to estimate irrigation for the field-scale data available for the Lleida region in this project. As can be seen from Fig. 10, most individual fields are much smaller than the pixel size of the irrigation dataset (500mx500m = 25ha).

Indeed, the average field only occupies an area of about 2 ha, although field sizes vary substantially with a standard deviation of 2.1 ha. Given that the field data is arranged in square clusters of approximately 700mx700m (Fig. 9), and that most clusters contain either only irrigated or only non-irrigated fields, it would seem reasonable to map irrigation on the cluster level.

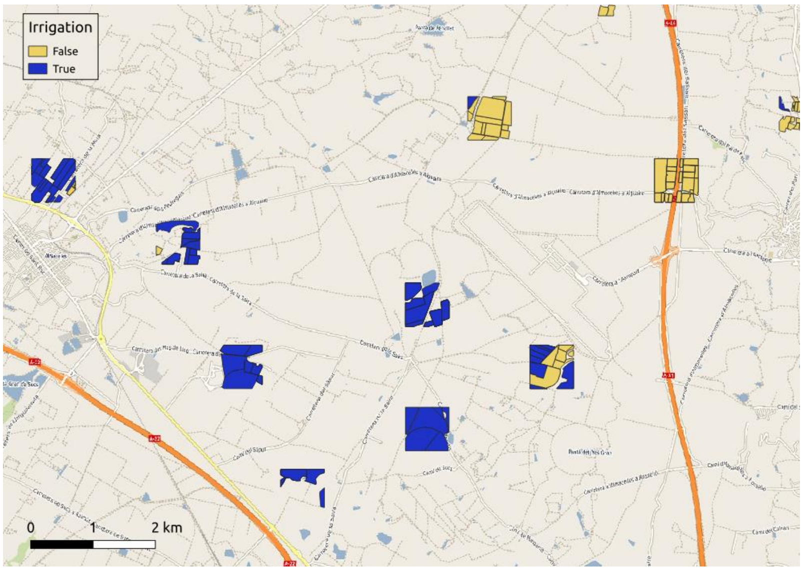

Figure 10: Exemplary map section of Lleida fields. Colours indicate whether the field is irrigated (blue) or not (yellow).

However, this would require all (or at least most) fields within a cluster to be used to cultivate the same crop or crops with the same growing – and therefore irrigation – season. Fig. 11 shows that this is not the case, as the summer crop maize is often grown on fields next to the winter crops barley and wheat. This will lead to erroneously mapped irrigation amounts. For example, if the same irrigation amount sometime in August from the irrigation dataset were mapped to all pixels in the cluster, one would wrongly conclude that a winter barley field was irrigated after the crop had already been harvested. Therefore, an algorithm was developed to map the pixel level irrigation data to the field-scale.

Figure 11: Exemplary map section of Lleida fields. Colours indicate the crop grown on each field.

This algorithm uses ancillary field-scale data from the Geographic Information System for Agricultural Parcels (SIGPAC), which provides yearly maps of all agricultural fields and their exploitation in all of Catalonia (https://agricultura.gencat.cat/ca/ambits/desenvolupament-rural/sigpac/mapa-cultius). The dataset provides information on the crop type of each field and whether it is irrigated or not. It is largely consistent with the field data provided to us. Newer versions also include information on the presence of double crops (typically winter barley followed by maize or corn), but this information is not available for the period under investigation here (2017-2020). Therefore, we employ the NDVI peak detection method devised by Olivera-Guerra et al. (2023) to classify double crops. The method locates peaks in the smoothed annual Sentinel-2 NDVI time series after averaging over pixels falling within each field. If two peaks are detected within the right time intervals of the summer and winter cereal growing seasons, the field is classified as harbouring two consecutive (double) crops. Fig. 12 depicts the percentage of fields correctly classified (identical to the provided dataset), classified as double crops or wrongly classified (other). For the three most common crops, more than 90% of fields are either classified correctly or classified as double crops, which validates the applicability of the algorithm to our dataset.

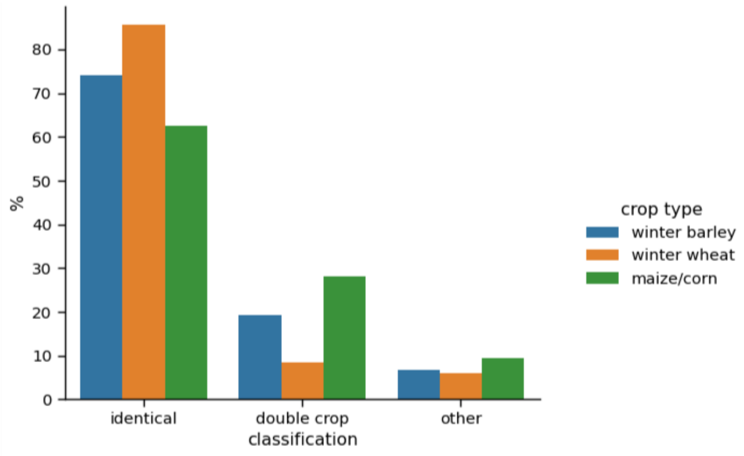

Figure 12: Crop type classification according to the NDVI peak detection algorithm for the three most common crop types.

The irrigation mapping algorithm proceeds as follows: For each irrigated pixel in the IRRIGATION+ dataset, the irrigation water amounts are resampled to monthly time intervals. Next, fields from the experimental dataset and the SIGPAC dataset falling into the pixel are selected and duplicates are removed. The total irrigation water volume V is then distributed amongst those fields according to $V = A\,h = \sum A_i\ h_i$,

where A and h are the total area of the pixel and the monthly total irrigation in mm, respectively. The quantities A_i and h_i denote the corresponding area and irrigation per field. Fields are assigned an irrigation weight w_i depending on the crop type, the month and whether the field is irrigated or not. This weight determines the amount of irrigation allocated to each field as $h_i = \frac{V\,w_i}{\sum A_j w_j}$.

For simplicity the following weights were chosen: $w_i = 0$ for all non-irrigated fields and for all winter and summer cereals outside their growing season; $w_i = 1$ for all irrigated fields with summer or winter cereals within their respective growing season; $w_i = 0.5$ for all irrigated fields with fruit trees or forages. Ideally, these weights should be calibrated with in-situ irrigation data, but this was beyond the scope of this project as such validation data was not available.

Fig. 13 depicts the total annual irrigation estimated via our mapping procedure for each year within the 2017-2020 period. These values are consistent with the originally retrieved per-pixel values, but equally underestimate total irrigation compared to district-scale reference data (see Zappa et al., 2021). Interestingly, our field-mapping approach shows greater differences in irrigation between crop types in different years than the original data. Winter wheat – and to a lesser extent, winter barley – were irrigated with far smaller amounts of water on average in 2018 compared to other years. As that year saw heavy rainfall in April and May, we would expect less need for irrigation of the winter cereals, while maize should not be affected by this, since its growing season doesn't start until June/July.

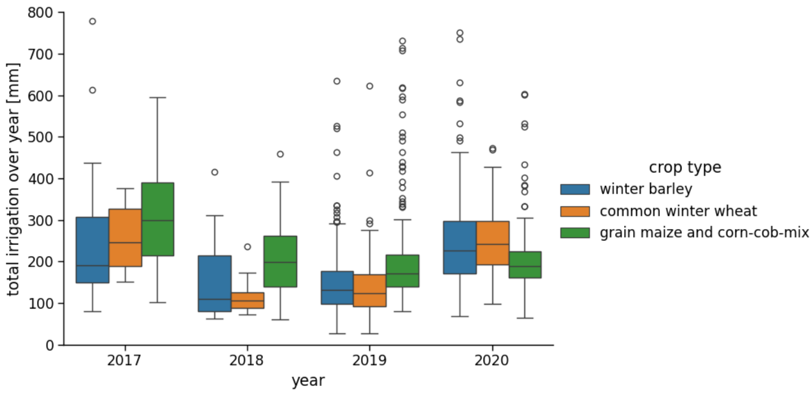

Figure 13: Total annual irrigation for different years in the observed period, colored by crop type.

As a next step, the impact of the irrigation amounts on crop yield was investigated. As can be seen from Fig. 14, the total annual irrigation has no measurable effect on the amount of crop harvested at the end of the season (pearson correlation not statistically significant for any of the crops). This might be due to the fact that the majority of the parcels in our dataset lie within the Urgell irrigation district, in which farmers predominantly utilize flood irrigation to water their crops. This system is characterised by fewer irrigation events with large amounts of water (which are difficult to precisely control), compared to drip or sprinkler systems. Numerous fields in the Urgell district furthermore feature drainage systems, resulting in surface runoff which is not considered in the SM_Delta method and thus leads to a likely underestimation of irrigation. Taken together, these caveats suggest that irrigation timing might play a bigger role for improving crop production in this region and will be investigated in the coming months (as part of the demonstration case 3: irrigation advisory tool).

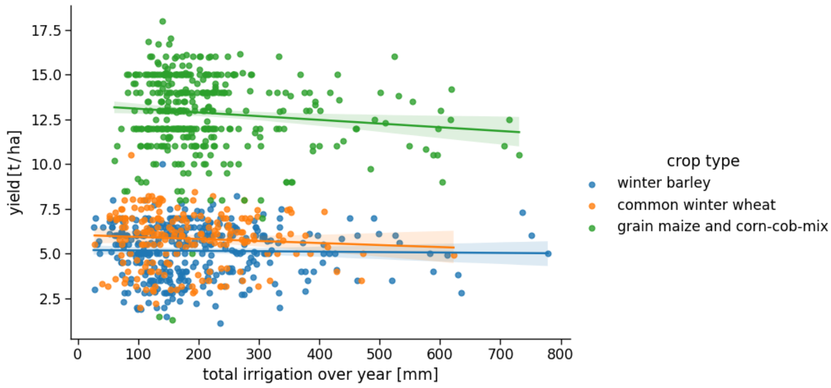

Figure 14: Total annual irrigation and yield at harvest for the three dominant crops.

To validate the irrigation amounts and timings that have been extracted with our newly developed irrigation mapping algorithm, they will be used as inputs to crop growth models and their output compared to the observed yield.

Bibliography

Isidoro, D., & Aragüés, R. (2007). River water quality and irrigated agriculture in the Ebro basin: An overview. Water Resources Development, 23(1), 91-106. https://doi.org/10.1080/07900620601159743

Olivera-Guerra, L. E., Laluet, P., Altés, V., Ollivier, C., Pageot, Y., Paolini, G., ... & Merlin, O. (2023). Modeling actual water use under different irrigation regimes at district scale: Application to the FAO-56 dual crop coefficient method. Agricultural Water Management, 278, 108119. https://doi.org/10.1016/j.agwat.2022.108119

Quast, R., Wagner, W., Bauer-Marschallinger, B., & Vreugdenhil, M. (2023). Soil moisture retrieval from Sentinel-1 using a first-order radiative transfer model—A case-study over the Po-Valley. Remote Sensing of Environment, 295, 113651. https://doi.org/10.1016/j.rse.2023.113651
Quiroga, S., Fernández-Haddad, Z., & Iglesias, A. (2011). Crop yields response to water pressures in the Ebro basin in Spain: risk and water policy implications. Hydrology and Earth System Sciences, 15(2), 505-518. https://doi.org/10.5194/hess-15-505-2011

Zappa, L., Schlaffer, S., Bauer-Marschallinger, B., Nendel, C., Zimmerman, B., & Dorigo, W. (2021). Detection and Quantification of Irrigation Water Amounts at 500 m Using Sentinel-1 Surface Soil Moisture. Remote Sensing. 13(9), 1727. https://doi.org/10.3390/rs13091727

Zappa, L., Dari, J., Modanesi, S., Quast, R., Brocca, L., De Lannoy, G., ... & Dorigo, W. (2024). Benefits and pitfalls of irrigation timing and water amounts derived from satellite soil moisture. Agricultural Water Management, 295, 108773. https://doi.org/10.1016/j.agwat.2024.108773

.1.4 Potential to give early indicators on yield for sugar beets for food processing stakeholders

This science case focuses particularly on supporting the food processing industry in planning and logistics. We will predict the expected yield of sugar beets at NUTS2 in the Netherlands which is the area in which the Cosun Sugar beet Company is active. We will also include sugar beet yields at the NUTS3 and field level from the Czech Republic. Yield of sugar beets is not only the tonnes per hectare, but the amount of sugar in the beet is also of high interest to the farmer and food processor. Therefore, in this case, we will investigate the relation between the available variables in the experimental datasets and sugar content in the beets provided by the farmers in the Netherlands and the Czech Republic. This will address one of the current science questions still open, if there is potential in predicting sugar content in beets with EO data.

Within this science case, two different crop growth models—Daisy and Hermes—were used at the field level for the experimental site of Polkovice farm in the Czech Republic (Fig. 15). Both models are used to test the accuracy of yield prediction at the field level with various weather or climate predictions. The amount of yield for sugar beet was observed from 2019 – 2023 at small experimental plots (at large experimental plots, the sugar beet was grown only for one year - 2021, according to the sowing practice).

Figure 15: Polkovice farm site with small experimental plots (36,5 x 52 m) and large experimental plots (252 x 150 m).

Daisy is a 1-dimensional agroecosystem model that, in brief, simulates crop production, crop yield, and water and nitrogen dynamics in agricultural soil based on information on management practices and weather data. The model can be viewed as an ensemble of processes, and to apply the model, the process models must be initialized and parameterized (Abrahamsen, Hansen, 2000). Input data for the Daisy model create 1. climate data – temperature, global radiation, precipitation, potential evapotranspiration, and groundwater level. 2. management and plant information – soil tillage, fertilization, irrigation, sowing, and harvest, species, and in-situ phenology.

The observed and subsequently simulated yield values are recalculated as dry matter in tons per hectare (for both Daisy and Hermes). The accuracy of the models is described with mean bias errors (MBE) and root mean square errors (RMSE); the MBE moved in 0 – 2.2 t/ha, and RMSE moved in 4.1 – 5.4 t/ha (Tab. 4). The biggest difference between observed and simulated is visible for the Daisy and Hermes models in 2019, where the actual yield was relatively low, and both models overestimated the amount of yield (Fig. 16, 17). For the other years (2020-2023), both models underestimate the yield (the Daisy model is slightly more intense), but this underestimate is acceptable in the case of sugar beet. Both models were calibrated according to all phenological data, and the current parameter settings for sugar beet best represent the climatic and pedological conditions in experimental site Polkovice.

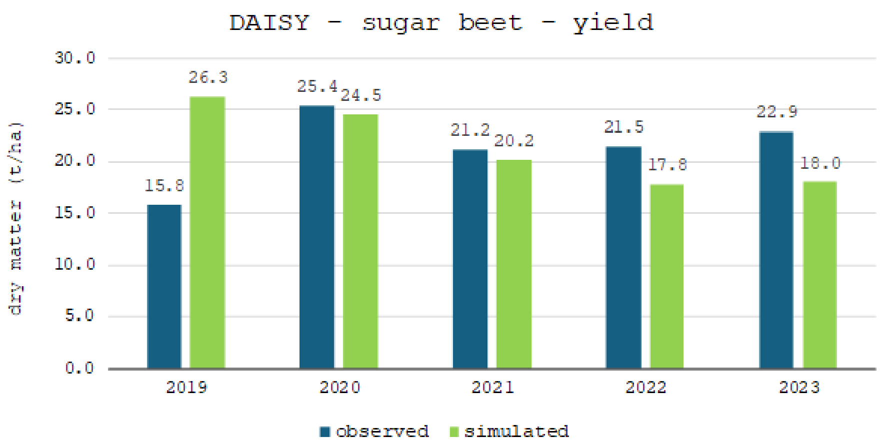

Figure 16: The observed and simulated yield (dry matter, t/ha) of sugar beet on Polkovice farm using Daisy model.

Table 4: Statistical values (MBE – Mean Bias Error and RMSE – Root Mean Square Error) for sugar beet using Daisy and Hermes models in dry matter (t/ha).

	Daisy		Hermes	
	MBE t/ha	RMSE t/ha	MBE t/ha	RMSE t/ha
Sugar beet	0	5.4	2.2	4.1

The HERMES model belongs among the widely used, easily accessible and well-documented crop growth simulation models (e.g. Kersebaum, 2008; Palosuo et al., 2011). It is a process-oriented model for estimating development and growth of the field crops, soil water balance and the dynamics of nitrogen for arable land. The benefit of using HERMES is the ability to work with a relatively small amount of input data sets that are ordinarily available at the farm level and that take into consideration plant growth, N-uptake, the process of net mineralization, the denitrification and transport of water and nitrate (Kersebaum et al., 2011). The sub-model for crop growth was developed on the basis of the SUCROS model (van Keulen et al., 1982). According to Kersebaum (2011), field capacity, wilting point and porosity may either be provided directly or applied from the stone content, texture and bulk density classes by German soil taxonomy. The input data can be divided into the following three parts: weather data, soil information and management data. Individual parameters entered into the model are obtained from soil and meteorological measurements including data about global solar radiation, air temperature (average, minimum and maximum), air humidity, wind speed, precipitation and tillage. Further, data of harvest, pre-crop and initial conditions are used to launch the model. The Penman-Monteith approach for estimating reference evapotranspiration is used (Allen et al., 1998, Monteith, 1965). The dynamics of soil water is derived from a simple capacity approach.

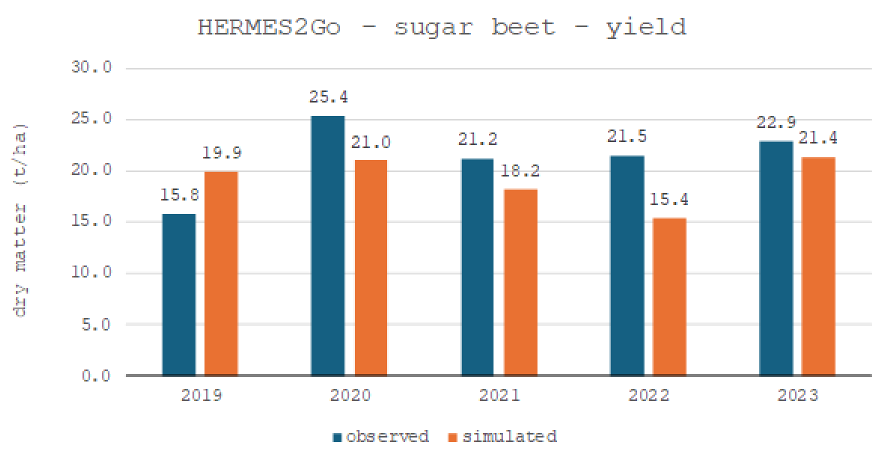

Figure 17: The observed and simulated yield (dry matter, t/ha) of sugar beet on Polkovice farm using the Hermes model.

The first step was to train both models. Specific weather or climate forecasts will be used to test both models' yield predictions in the following steps. We used the M&Rfi (Rötter et al. 2011), a single-site weather generator, and an improved version of Met&Roll (Dubrovsky et al., 2000, 2004). M&Rfi was trained for the Polkovice farm to calculate various weather forecasts to test the accuracy of yield predictions by both models (Daisy and Hermes). We will use four different types of prediction in monthly time steps from March to July. The first version will use only observed weather data; the second version will use the outputs from M&Rfi with weather data, which will be calculated with random variability; the third version will use again the outputs from M&Rfi with weather data, which will be calculated on the base of long term averages; the last version will be based on real seasonal forecast which will be used as input for M&Rfi to simulate the weather forecast. This approach allows us to evaluate the accuracy of yield prediction in different time steps before the harvest and also with different weather/climate predictions.

Both models (Daisy and Hermes) are calibrated with in-situ data observed properly during the whole vegetation season in each year (including e. g. detailed phenological observations, information about soil and soil moisture properties and weather conditions). Accurate modeling at the field level then allows us to compare the modeled values with remote sensing data (e.g., Leaf Area Index - LAI) and verify the correct use of RS data. Further work with RS data must, therefore, be preceded by precise modeling at the field level with detailed knowledge of the input site conditions. For this reason, the first simulations were carried out in the Czech Republic, where we had good-quality data for the field level together with other parameters (e.g., detailed information about phenological phases during vegetation periods, which helped to refine the modeling), without exact modeling would not be sufficient. Modeling at the field level can then be compared not only with RS data but also with spatial modeling, which we are able to do in the Czech Republic. There, we have sufficient data not only at the field level but also long enough series for modeling at the regional level (NUTS3).

Besides the crop growth models (Daisy and Hermes), we also used an optimized neural network for the prediction of yield for sugar beet on the NUTS3 level within the area of the Czech Republic. The outputs are available online (only in the Czech language) at the website www.vynosy-plodin.cz in weekly time step (not only for sugar beet but also for other crops such as spring barley, winter wheat, winter rape, maize, oats, and rye).

40 potential input characteristics were selected for yield prediction. In addition, data for the period 2000 – 2018 are available from the Moderate Resolution Imaging Spectroradiometer (MODIS) carried by the Terra satellite, which captures 250 m resolution of the Earth's surface in a daily step.

For final yield prediction, various predictors were used – vegetation indices, soil water index (SWI), evaporative stress index (ESI), and various outputs from the model SoilClim.

According to the vegetation indices the NDVI, EVI, and EVI2 were used.

SWI quantifies the soil moisture status in different soil depths. The index value is calculated based on an algorithm based on an infiltration model describing the relationship between Surface Soil Moisture (SSM) and soil moisture profile as a function of time (Wagner et al., 1999). The SSM used for the SWI calculation is obtained from the ASCAT sensor on board the MetOp-A and MetOp-B satellites, for daily values are used for the calculation. The resulting daily SWI data is then provided as part of the service Copernicus. Weekly averages of SWI are then used for the actual prediction. Excluded from the calculation are areas of water, permafrost and snow cover.

The ESI (Evaporative Stress Index) expresses the time-standardized anomaly of the ratio of the current and reference evapotranspiration (ETa/ETo). The determination of ETa is performed using a diagnostic model ALEXI (Atmosphere-Land Exchange Inverse model), which has a two-source (soil and vegetation) energy balance model. In the framework of the present methodology, the surface temperature measured for the ALEXI model was chosen. MODIS sensors carried by the Aqua and Terra satellites with a spatial resolution of 0.05° (i.e. 5 km at the equator). Other necessary input data are meteorological variables from 2 m above the surface (temperature, pressure and humidity and wind speed), for which the CFSR (Climate Forecast System Reanalysis) was used. Additional data is albedo (MODIS-Terra - required for the determination of the element's radiation balance, including heat flux to the soil) and approximate aerodynamic surface roughness based on height vegetation.

The quantification of the individual components of the water balance using the SoilClim model is a significant input for yield forecasting, as it allows the inclusion of the water stress factor, different soil and terrain conditions and also complements the satellite information with information from ground stations in a relatively reliable way. The SoilClim model, which was developed in the framework of the cooperation between the Institute of Agrosystems and Bioclimatology at Mendel University in Brno and the present Institute of Global Change Research of the CAS, v.v.i. and other institutes, was used to determine soil water supply for yield prediction purposes (Hlavinka et al., 2011). The software has a modular structure, with the key parts being input meteorological data in daily time steps, reference evapotranspiration, snow cover model, vegetation, and soil parameters.

For sufficient robustness in estimating crop yields, this methodology works with two procedures to derive the functional relationship between the predictors and crop yields, which are then used in the aggregate model ensemble.

The first part creates the neural network modeling. The yield forecast with neural network is done in weekly steps, starting from the 13th week of the year. Separate neural networks were created for each week of the year, each crop, and each territorial unit (NUTS3 region). Each neural network, therefore, solves one specific task, e.g., the prediction of sugar beet yields for the NUTS3 in week 20. The cumulative values of the selected characteristics were used as inputs from data for the week of the year (e.g., for the week 20 prediction, the values for weeks 1 to 19 are known). The values of yields in a given year were used as output. The patterns thus generated were transmitted to the neural network, of which ¾ were used to learn the network and the rest to test the network's usability. For yield prediction, 50 networks were trained for each variant (NUTS3, crop, week), and 30 networks with the best prediction ability were selected for generating yield estimates. The result of the prediction is the average, 5th and 95th percentile of the results from the selected 30 networks.

The next part creates linear models. Remote sensing data were used as a predictor data from the MODIS sensor carried by the Terra satellite, which are available for the study area in the time series from the year 2000. From the original daily image data with global coverage in 250 m spatial resolution, weekly NDVI and EVI2 vegetation index data were prepared as maxima per week and aggregated only for the arable land of the given spatial unit (NUTS3). The single linear regression was used because a short time series of actual yield was available (incomplete data series since 2000). Pairs of the selected vegetation index values and the actual yield are entered into the forecasts for a given NUTS3. From the weekly data, suitable continuous periods are selected to indicate the course of the season (none of the weeks between the first and the last selected are omitted), for which the values from each week are averaged into a single value. Selection of the most appropriate period, for which the observed index values are most indicative of the subsequent level of yields, is based on comparing the predictive ability of all possible linear models, and a specific analysis was carried out using a 'leave-one-out' procedure.

To avoid significant errors in a model, using multiple models and considering some combination of these models as the final estimate weighted average is appropriate. In our case, we have two models. The final forecast of yields is presented as the result based on the best linear model and the average of the ensemble of neural networks for a given date, as the average of the two models. Thus, both models weigh one-half.

The website provides various outputs about yield prediction for sugar beet. Firstly, users can check the yield prediction (Fig. 18, left side) in tons per hectare in the weekly time step and compare it with prediction reliability in percent (Fig. 18, right side). The yield prediction could also be compared with deviation from the average yield of the previous year (Fig. 19, right side) or with observed and estimated drought impacts on yield (Fig. 20, right side).

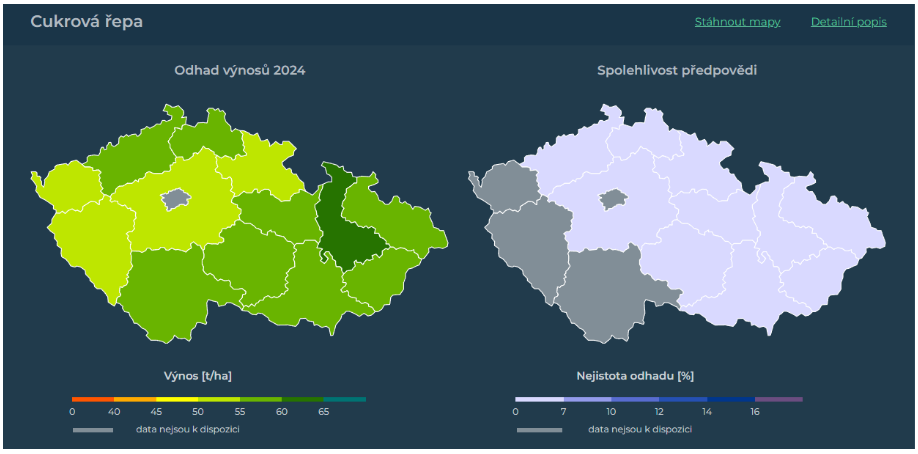

Figure 18: The real yield prediction for sugar beet in tons per hectare on the left side. With prediction reliability in % on the right side.

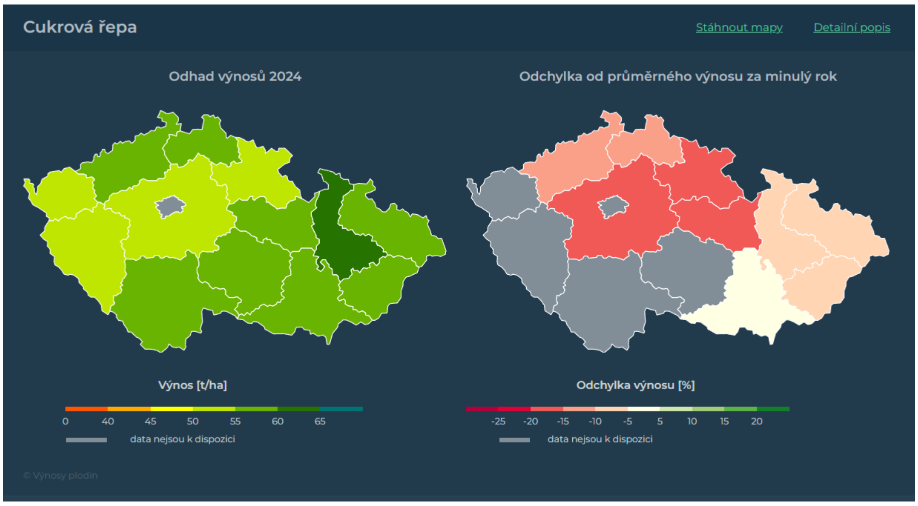

Figure 19: The real yield prediction for sugar beet in tons per hectare on the left side. With deviation from the average yield of the previous year in % on the right side.

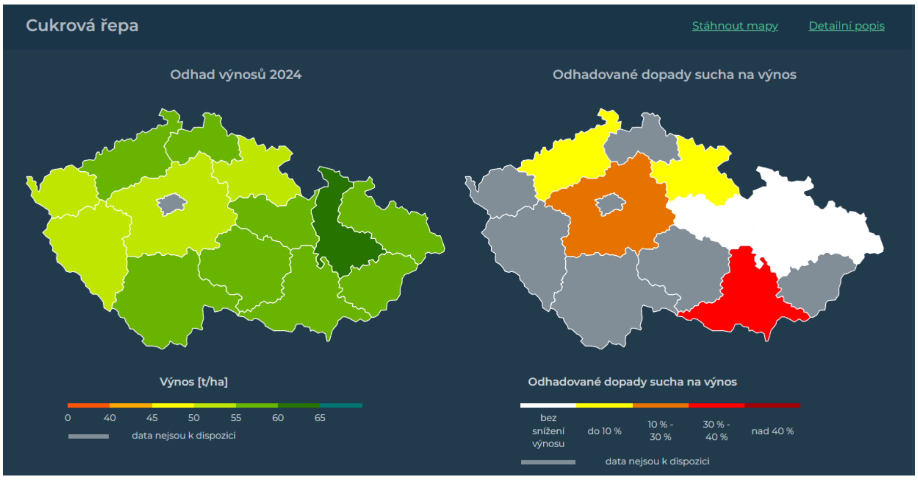

Figure 20: The real yield prediction for sugar beet in tons per hectare on the left side. With estimated drought impacts on the expected yield during the vegetation season on the right side.

Bibliography:

Dubrovsky M, Zalud Z, Stastna M (2000) Sensitivity of ceres-maize yields to statistical structure of daily weather series. Clim Change 46:447–472.

Dubrovsky M, Buchtele J, Zalud Z (2004) High-frequency and low frequency variability in stochastic daily weather generator and its effect on agricultural and hydrologic modelling. Clim Change 63:145–179.

Hlavinka P, Trnka M, Balek J, Semerádová D, Hayes M, Svoboda M, Eitzinger J, Možný M, Fischer M, Hunter E, Žalud Z (2011) Development and evaluation of the SoilClim model for water balance and soil climate estimates. Agricultural Water Management 98(8): 1249-1261.

Kersebaum KC (2007) Modelling nitrogen dynamics in soil-crop systems with HERMES. Nutrient Cycling in Agroecosystems 77,39–52.

Kersebaum KV (2011) Special Features of the HERMES Model and Additional Procedures for Parameterization, Calibration, Validation, and Applications. Book Series:Advances in Agricultural Systems Modeling. Methods of Introducing System Models into Agricultural Research, Volume 2 https://doi.org/10.2134/advagricsystmodel2.c2.

Palosuo T, Kersebaum KC, Angulo C, Hlavinka P, Moriondo M, Olesen J, Patil R, Ruget F, Rumbaur C, Takac J, Trnka M, Bindi M, Caldag B, Ewert F, Ferrise R, Mirschel W, Saylan L, Siska B and Rötter R (2011) Simulation of winter wheat yield and its variability in different climates of Europe: a comparison of eight crop growth models. European Journal of Agronomy 35, 103–114.

Rötter RP, Palosuo T, Pirttioja NK, Dubrovsky M, Salo T, Fronzek S, Aikasalo R, Trnka M, Ristolainen A, Carter TR (2011) What would happen to barley production in Finland if global warming exceeded 4 °C? A model-based assessment. Europ J Agronomy 35:205–214.

Van Keulen, H., FWT Penning De Vries, and E. M. Drees. "A summary model for crop growth." *Simulation of plant growth and crop production*. Pudoc, 1982. 87-97.

Wagner W, Lemoine G, Rott H (1999) A method for estimating soil moisture from ERS scatterometer and soil data. Remote Sensing of Environment, 70, 191-207.

2. Societal Impact

.2.1 Subfield and field-level yield forecasts with lead time of at least 4 months including several crops (CG-A)

The subfield and field-level forecats were prepared at site Polkovice (Fig. 15) for three main crops – winter wheat, winter rape and spring barley at large experimental plots (252 x 150 m). The accuracy of the subfield and field level yield forecasting is based on a good-quality input data and all specific inputs which influnced the vegetation season (e.g. pests, diseases, specific management inputs) and finally the yield in each year. All these specific information were collected at the mentioned site for large experimental plots were given crops were grown since 2019. For the testing of yield prediction accuracy the crop growth models were used – Daisy and Hermes (details in chapter 0.1.4 above).

For winter wheat and winter rape the yield data are missing for two specific years (2020 and 2021) because of the original crop has been replaced by spring wheat (in case of winter wheat in 2021) and by soya (in case of winter rape in 2020). Nevertheles the Daisy model can predict the winter wheat yield and reflect local conditions sufficiently (Fig. 16) and the expected error is expressed by RMSE (Root Mean Square Error) and MBE (Mean Bias Error) (Tab. 5) moving in -1.6 t/ha (MBA) and 2.7 t/ha (RMSE). The visible difference in observed and simulated yield in 2019 is caused by vole who destroyd the whole yield, still the models reflect given conditions and predict the yield without this disturbance.

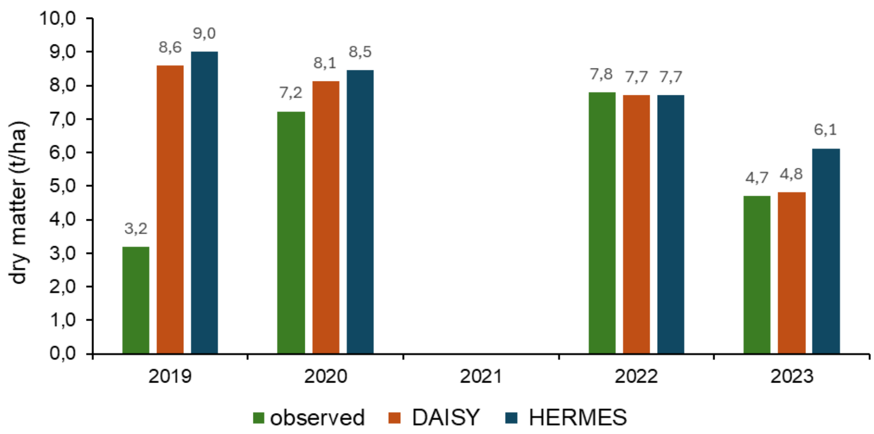

Figure 16: The observed and simulated yield (dry matter, t/ha) of winter wheat on Polkovice farm using Daisy and Hermes model.

Table 5: Statistical values (MBE – Mean Bias Error and RMSE – Root Mean Square Error) for given crops using Daisy and Hermes models in dry matter (t/ha).

	Daisy		Hermes	
	MBE	RMSE	MBE	RMSE
	t/ha	t/ha	t/ha	t/ha
Winter wheat	-1,6	2,7	5,7	6,0
Winter rape	-0,2	0,5	4,3	4,4
Spring barley	-1,9	2,7	5,0	5,3

For other crops (winter rape and spring barley) still the Daisy model can evaluate the given condition better (Fig. 17 and 18) according to the Hermes model (since the values of RMSE and MBE are lower for Daisy model, Tab. 5). In the future the accuracy of the yield prediction will be further tested using various types of meteorological forecats.

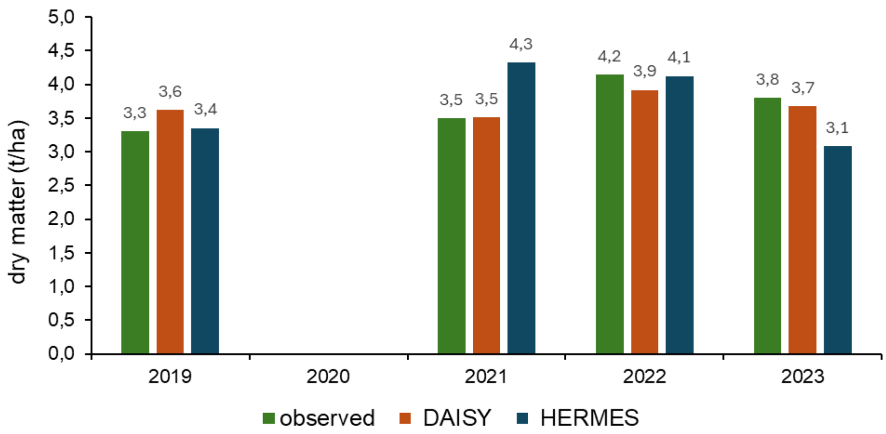

Figure 17: The observed and simulated yield (dry matter, t/ha) of winter rape on Polkovice farm using Daisy and Hermes model.

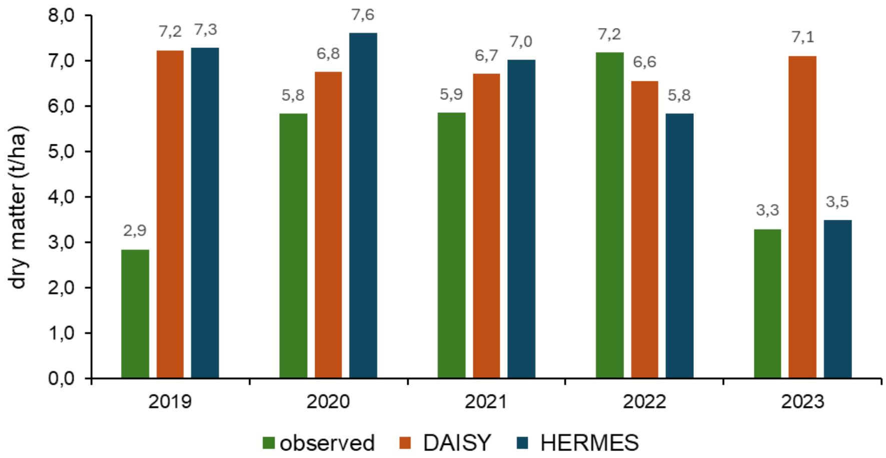

Figure 18: The observed and simulated yield (dry matter, t/ha) of spring barley on Polkovice farm using Daisy and Hermes model.

For yield prediction not only the crop growth models could be used. On the NUTS4 level we also used the neural networks and linear models for given crops and published the outputs online on website www.vynosy-plodin.cz. The detailed methodology is described in chapter 0.1.4. The yield prediction was calculated for the period 2017-2024 and is updated every once a week (always on Monday afternoon when the meteorological data are download and evaluated from the last 7 days).

For each crop (winter wheat, winter rape and spring barley) the current prediction is calculated (based on described methodology) and additional information are added, such as the real amount of yield (the values are added during the vegetation season since the data are displayed by farmers), prediction realibility (based on estimation uncertainty in percentage), deviation from the average yield in the previous year, deviation from the average yield in the last 3 years, estimated drought impacts (as a factor whit high impact on the final yield) and the percentage of harvested areas (Fig. 19).

All the maps can be download with additional maps and information (such as 5 districts with the highest predicted yield and 5 districts with lowest yield predicted in given week etc.).

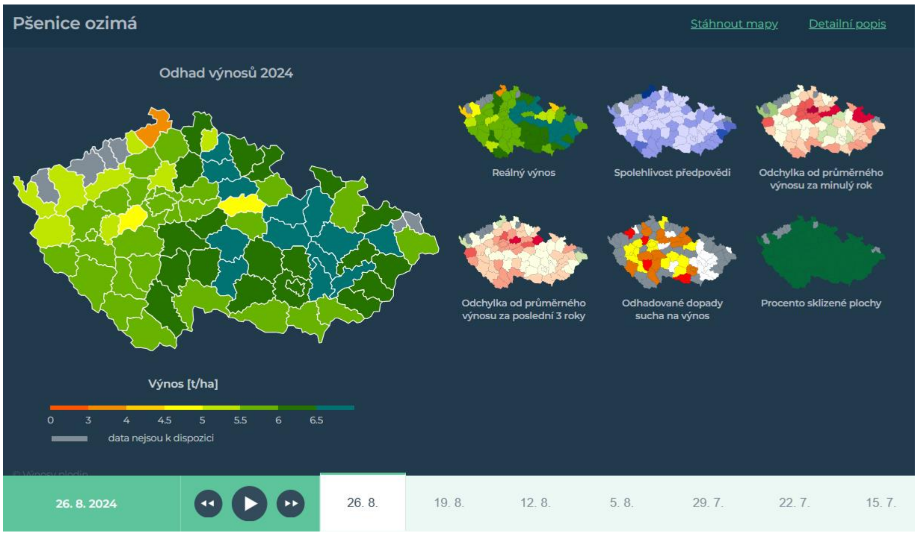

Figure 19: Example from vegetation period 2024 for winter wheat from the end of August when all the fields were harvested. The bigger map display the yield prediction, 6 small maps desribe the additional information (the real yield, prediction realibility, deviation from the average yield in the previous year, deviation from the average yield in the last 3 years, estimated drought impacts and the percentage of harvested areas.

At a workshop in February 2024, organized as part of the Yipeeo project activities, with farmers and stakeholders, the questionnaire survey revealed that farmers were sceptical about the yield forecast.

The uncertainty of the forecast, the effects of a large number of elements and the general inability to predict yield were often cited as reasons for not using yield forecasting. However, website traffic suggested tens and in some periods hundreds of visits per week (Fig. 20).

Figure 20: Number of active visitors of the website www.vynosy-plodin.cz during the year 2024.

.2.2 Retrospective yield prediction on different spatial scales level to quantify yield anomalies (TUW-RS)

1. Goals:

The goals of this demonstration case are: (1) To quantify yield losses before or shortly after harvest for compensation payments (insurance or nation agencies) on different spatial scales. As yield losses are a sensitive information we compare here the accuracies of models predicting yield at field scale and aggregate it to NUTS4 scale and a model predicting directly at NUTS4 scale. (2) Evaluate the impact of the lead time on different spatial scales. Here we also focus on field scale and NUTS4 scale.

2. Data:

For this demonstration we used the reference crop yields for winter wheat, spring barley, and maize in Czechia. This selection was based on the fact, that these crops are among the most cultivated crops in Europe and the data basis for Czechia ranged from field level to NUTS2 level. On field level, the data from the Polkovice farm and the Rostenice farm was used. The data from the Polkovice farm includes 32 samples for winter wheat, 40 samples for maize, and 40 samples for spring barley. Rostenice farm is significantly larger and includes 323 samples for winter wheat, 501 samples for maize (green maize and grain maize), and 448 samples for spring barley. For both farms the data covers the years 2016 to 2022. The fields from these farms are located in three different NUTS3 regions (NUT IDs: CZ0643000000, CZ0646000000, CZ0713000000). Based on the findings from previous tasks predictors with a high predictive power were selected. These were ERA5

SWI, ERA5 radiation, ERA5 radiation and the Sentinel-1 CR as well as the EVI derived from Sentinel-2.

The EO based predictors were available on field scale and aggregated to the NUTS4 level. Due to the coarser spatial resolution of the meteorological variables, the closest ERA5 grid cell for the centroid of the NUTS regions was identified.

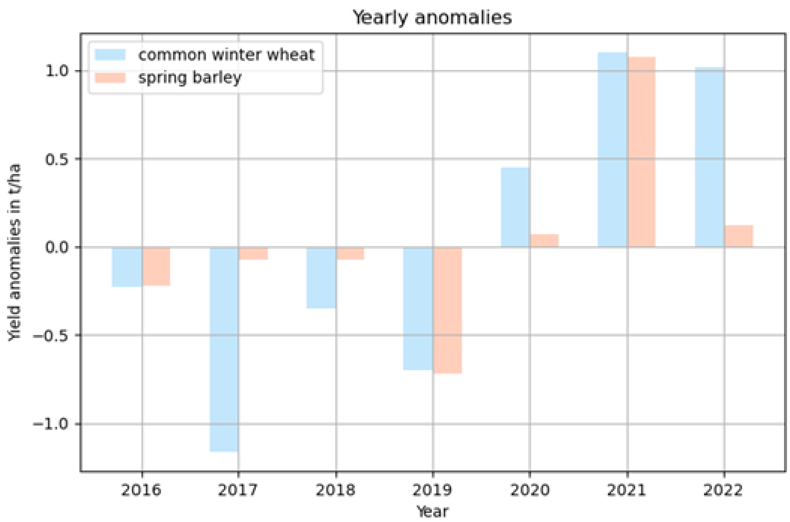

Figure 1: Yield anomalies for the years 2016-2022 for Winter Wheat and Spring Barley for the NUTS region CZ064000000.

Figure 1 illustrates the yield anomalies for the NUTS4 region CZ064000000 for winter wheat and spring barley and the years 2016-2022. For the years 2016-2019 both crops show negative anomalies, whereas for the years 2020-2022 both crops show positive anomalies. However, for some years significant differences can be observed: In 2017 and 2022 the anomaly for spring barley is much more extreme than for winter wheat. The increasing trend in yield can potentially be attributed to improvements in agricultural practices in recent years. The low yields in 2017 and 2019 on the other hand are most likely a result of below average precipitation in spring in these years.

3. Methodology:

The set-up of this demonstration case is closely aligned to task 3 and the associated deliverables ATB and product validation report. We used a Gradient Boost Regressor and a randomized grid search to identify the best parameters for the yield prediction models.

In the end, a GRU model with 250 estimators, a maximum depth of 3, and a learning rate of 0.025 was used. For the validation of the model, a leave one year out cross validation was used. Distinct models were trained per crop type and per lead time. The experiment for the estimation of yield losses was carried out with the data from the Rostenice and Polkovice farm and the NUTS4 region CZ0640000000. Due to the low number of regions on NUTS3/NUTS2 and national level, proper model training and testing was not possible. For this reason, no prediction was carried out on these scales.

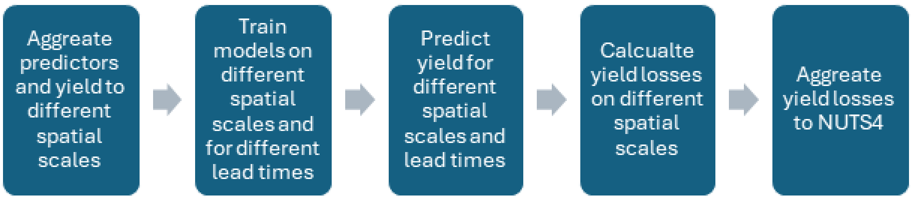

Figure 2: Workflow for the demonstration case illustrating the individual steps performed to achieve the results.

4. Results:

4.1. Quantification of yield losses on different spatial scales

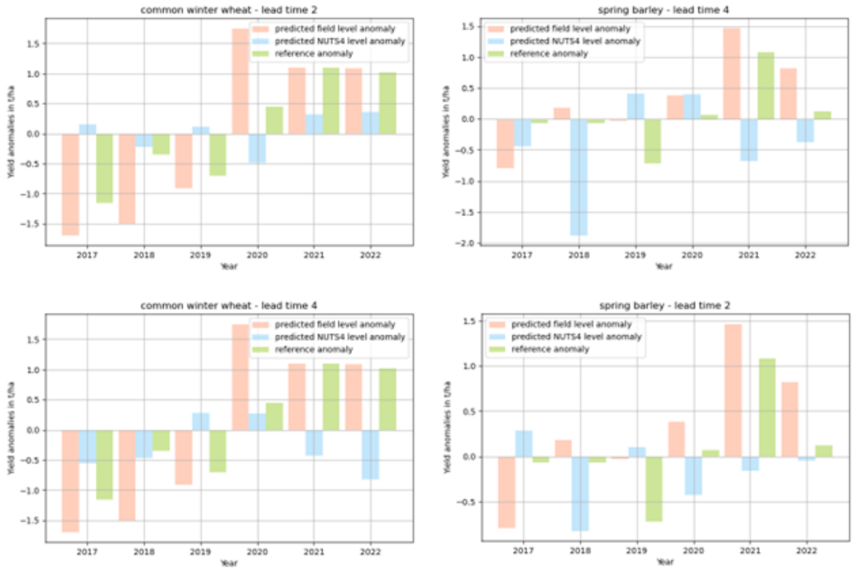

Figure 3: Derived yield anomalies aggregated from field level predictions to NUTS4 level and directly predicted on NUTS4 level for Winter Wheat and Spring Barley, lead times 2 (upper row), and 4 (lower row), all for the NUTS4 region CZ0646000000.

First, two approaches to estimate yield losses on NUTS4 level were compared. The first approach predicts yield on field level and then aggregates these predictions to NUTS4 level to calculate the yield loss by subtracting the average yield of this crop. The second approach predicts directly the yield on NUTS4 level and then calculates the yield loss in the same way as for the first approach. This experiment was carried out for the lead times from 1-4 months. Figure 3 illustrates the retrieved yield losses for the two approaches for all years and the crops common winter wheat and spring barley exemplary here for the lead time 2 month and 4 months. As can be seen from the figure, the deviation between the actual yield loss and the estimated yield loss for approach 1 (prediction at field level and aggregation to NUTS4 level) is smaller in most cases. For winter wheat, this applies for all years except for 2018 and 2020 (for both illustrated lead times). For spring barley, the same applies for all years except for 2017 and 2022. It is also evident that the model for the NUTS4 level has the tendency to underestimate yield anomalies. Similar trends are also observed for the lead times 1 and 3 which are not illustrated here.

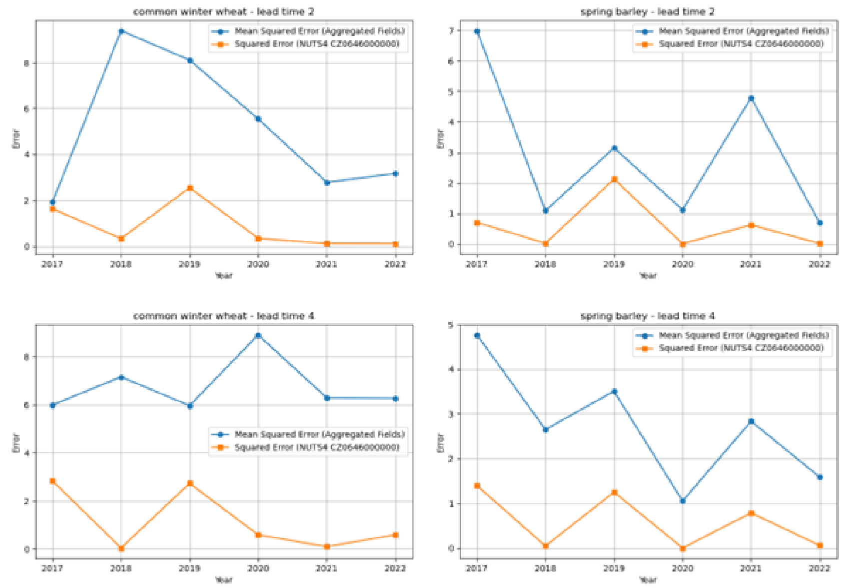

Figure 4: Comparison of error metrics of yield aggregated from field level predictions to NUTS4 level and directly predicted on NUTS4 level for Winter Wheat and Spring Barley, lead times 2 (upper row), and 4 (lower row), all for the NUTS4 region CZ0646000000.

In addition, we calculated also the mean squared error respectively squared error for the two approaches. For the prediction on field level, we used the MSE over all fields within the NTUS4 region CZ0640000000. For the prediction directly on NUTS4 level the squared error was calculated between the predicted yield for this NUTS4 region and the reference yield. Figure 4 illustrates the achieved metrics for this. As can be seen, in this case the metrics for the prediction directly on NUTS4 level are significantly better for both crops, both lead times and all years. A more detailed interpretation of the results is provided in the last chapter.

4.2. Yield prediction with different lead times on different spatial scales

In a next step, the impact of the lead time on the yield prediction accuracy on different spatial scales was assessed in detail. This was carried out on field level and on NUTS4 level, but this time no aggregation to NUTS4 level was performed. The analysis was done on sub-field level and field level for the crops winter wheat, spring barley and maize and on NUTS4 level for winter wheat and spring barley only, as no data on maize yield was available. Figure 5 illustrates the achieved RMSE on field level and NTUS4 level. As can be seen from the figure, the differences between the lead times are marginal or significant depending on the crop type and level. For maize at field level, the RMSE increases significantly with increasing lead time. The same applies to spring barley at field level. Winter wheat shows an almost identical trend for the different lead times at field and NUTS4 level, where only a slight increase in RMSE can be observed with increasing lead time. The same applies to spring barley at field level, and the differences between the lead times are only marginal.

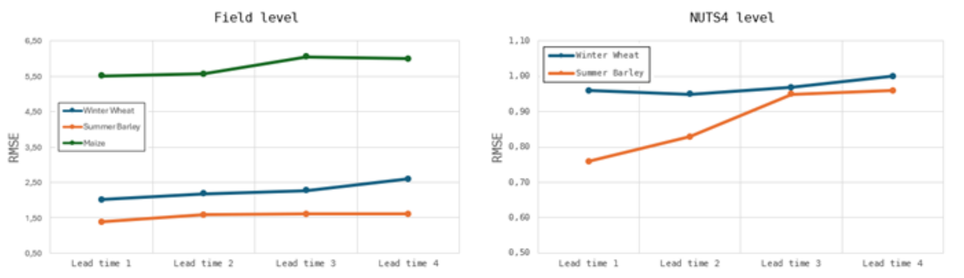

Figure 5: RMSE on field level (left) and NUTS4 level (right) for different lead times and the crops Winter Wheat, Summer Barley, and Maize averaged over all years where data was available. The RMSE is the weighted averaged over all available years.

In addition we also took closer look at the yearly performance for different lead times. This is illsutrated in Figure 6. As can be seen, the differences between the years are significant, especially for winter wheat. There are two years (2017 and 2020) where the RMSE for lead time 1 is actually the highest. For spring barley, on the other hand, lead time 1 has the lowest RMSE in all years and lead time 4 has the highest RMSE in all years except 2016.

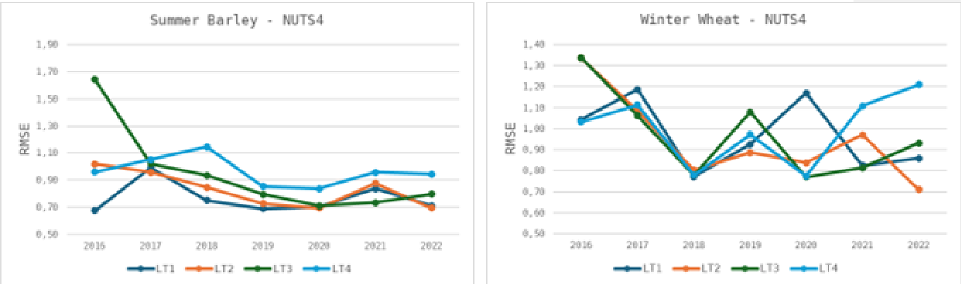

Figure 6: RMSE on NUTS4 level for the crop Summer Barley and Winter Wheat and the lead times 1-4 for different years.

Tables 1 and 2 summarize the achieved accuracy metrics for the different spatial scales. It can be seen that a lower accuracy was achieved on field level. For winter wheat and spring barley, accuracies are significantly lower for all lead times. Only for maize, accuracies for lead time 1 and 2 are close to the field level.

Field Level

Table 1: Summary of the achieved metrics for yield prediction on field level for the crops Winter Wheat, Spring Barley, and Maize and the lead times 1-4.

Crop	Lead time	RMSE (t/ha)	MAE (t/ha)	PearsonR
Winter Wheat	1 2 3 4	2.02 2.18 2.27 2.59	1.80 1.98 2.06 2.43	0.17 -0.30 -0.07 -0.11
Spring Barley	1 2 3 4	1.39 1.59 1.60 1.61	1.15 1.34 1.37 1.36	0.22 0.28 -0.03 0.05
Maize	1 2 3 4	5.52 5.58 6.06 5.97	3.05 4.03 3.55 3.73	0.28 0.14 0.27 -0.01

NUTS4

Table 2: Summary of the achieved metrics for yield prediction on field level for the crops Winter Wheat and Spring Barle and the lead times 1-4.

Crop	Lead time	RMSE (t/ha)	MAE (t/ha)	PearsonR
Winter Wheat	1 2	0.97 0.95	0.77 0.77	0.15 0.21

	3	0.97	0.78	0.13
	4	1.00	0.81	-0.02
Spring Barley	1	0.76	0.61	0.48
	2	0.83	0.68	0.46
	3	0.95	0.78	0.29
	4	0.96	0.78	0.17

5. Discussion and conclusion:

The outlined results indicate, that yield prediction on field scale is more challenging, than on regional (NUTS4 scale). A driving factors for this could be the higher variance of the yield on field scale that can not (fully) be explained by the used predictors. Other factors like soil types, nutrition supply, hail or pest related yield losses are not represented in the predictors but can have a high impact on field level. Aggregated yield predictions from field level to NUTS4 level however have shown to give a good approximation of average yield on NUTS4 level and outperformed a prediction on NUTS4 level in most years. The main explanation for this difference is, that during the aggregation to NUTS4 level errors from under- and overpredictions on field level are averaged out. It must be taken into account that this is based on an analysis of only one NUTS4 region. A general statement if this approach is advantageous is thus difficult. With regards to the impact of the lead time, a general statement is also difficult. Only spring barley on NUTS4 level showed in our analysis a clear trend with increasing RMSE with increasing lead times and lead time 1 having the lowest RMSE in all years. For winter wheat, the differences between the years were so extreme that a general statement is not possible.

.2.3 Irrigation advisory tool (TUW-C)

The aim of this demonstration case was to assess how the yield predictions, the irrigation information on the field scale and the irrigation estimation from Earth Observation data (Science Case 3) could be combined to develop an irrigation advisory tool that could be used by stakeholders. Ideally, it would alert them in time to potential yield losses due to low water availability and advise them on how to mitigate those losses through the application of irrigation.

As a first step towards this goal, we assessed whether the machine learning model developed in Task 3 was able to correctly predict the yield differences between irrigated and non-irrigated fields in the Lleida and Madrid regions of Spain. As predictor variables, we extracted timeseries of Sig0/Sig40 VV, VH, and CR from Sentinel-1, as well as the calculated indices NDVI, EVI, NMDI, NDWI from Sentinel-2 and resampled them to a biweekly resolution. We established eight crop yield forecasts at different times before the harvest of each particular crop. Each of these forecasts are two weeks apart, starting at four months before harvest and ending at two weeks before harvest. These forecast times are denoted LT (lead time) 8 to 1, with LT8 meaning 8 times 2 weeks before harvest, i.e. 4 months. The forecasts are always started at LT8, such that subsequent forecasts (and their training) can take the previous forecasts into account as additional predictor variables. We employed a machine learning model based on Extreme Gradient Boosting and optimized the hyperparameters with a randomized grid search.

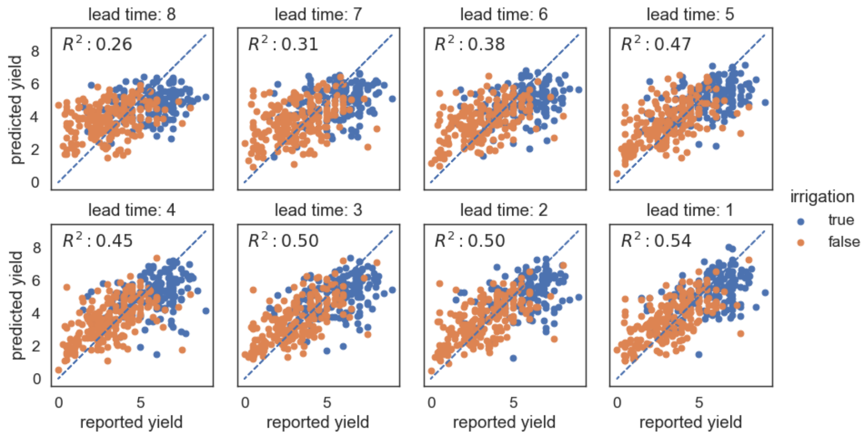

Figure 1: Predicted and reported yield for irrigated and non-irrigated fields of common winter wheat at different lead-times (in biweekly intervals).

First, as the machine learning model developed in Task 3 was never tested on the data from the Lleida and Madrid regions before, we assessed how well it was able to predict yield at different lead times overall. Figure 1 compares the predicted yield with the reported yield for all fields in the testing set and clearly shows that the R^2-score, corresponding to the explained variance of the data by the model, gradually increases as the forecasts move closer to the harvest, and that the forecasts already yield sensible results around 10 weeks (LT5) before harvest. Furthermore, a visible distinction between irrigated and non-irrigated fields is established in the predictions and gets stronger as the harvest approaches.

This effect is illustrated and quantified in more detail in Figure 2, which depicts the distribution of predicted yields for both irrigated and non-irrigated fields at different lead times, as well as the reported yields. At 4 months before harvest, the two distributions are fairly similar, but they drift apart continuously as the harvest approaches, with irrigated fields gradually being forecast to have increasing yields, whereas the forecasted yields of non-irrigated fields decline over time. It should be noted, however, that irrigated and non-irrigated fields already show some differences at the earliest lead time, before irrigation could have had any effect. This might be because many irrigated fields are clustered in the main irrigation districts and thus are not subject to the exact same environmental conditions as the fields that lack irrigation.

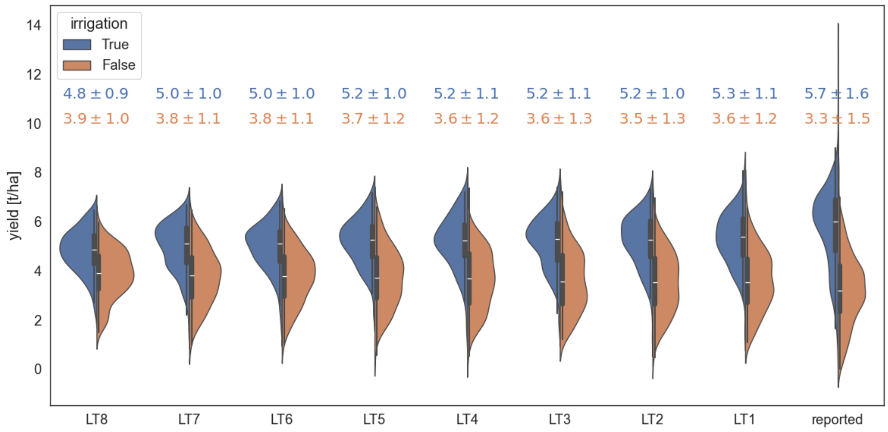

Figure 2: Distribution of predicted yields for irrigated and non-irrigated fields of common winter wheat at different lead-times (in biweekly intervals). The reported yield is shown as a reference. Numbers above violin plots indicate the mean and standard deviation of the distributions.

As such, we tried to further compare individual fields by finding spatial matches between irrigated and non-irrigated fields which are less than one kilometer apart. For such closely situated fields, we can safely assume that external conditions, such as soil properties, altitude or weather conditions, are identical or at least similar enough to make irrigation the main driver of any predicted differences in yield.

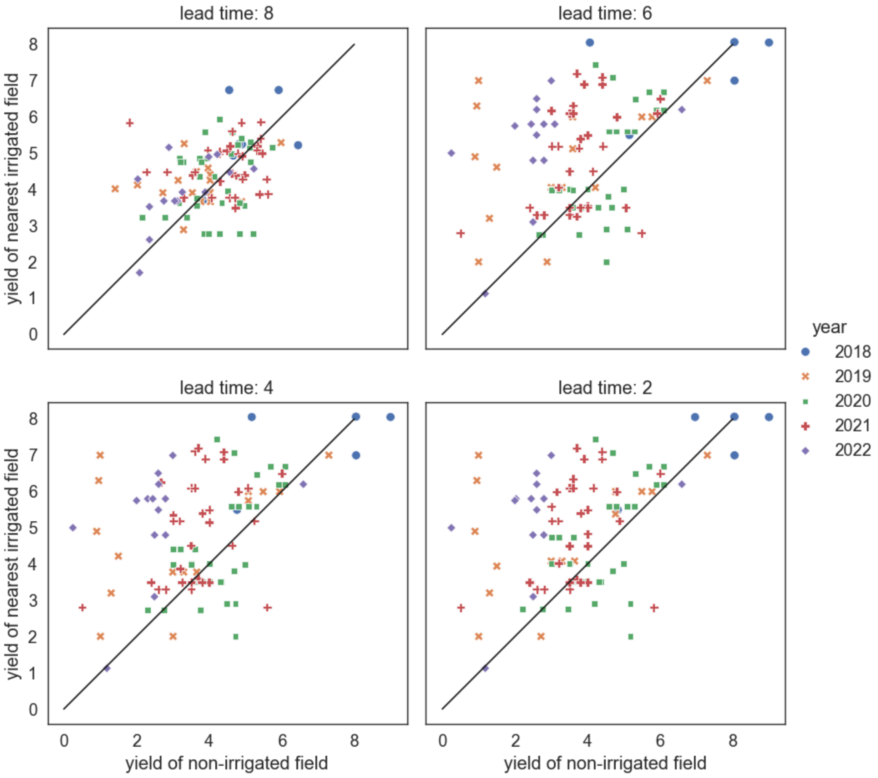

Figure 3: Comparison of predicted yield for pairs of non-irrigated fields and their closest irrigated fields of common winter wheat at different yield times. The marker types and colors correspond to different years.

Figure 3 compares the predicted yields for these spatially matched pairs at four different lead times, corresponding to four, three, two and one months before harvest, respectively. The datapoints are colour coded by year to allow us to connect the effects of irrigation with the weather conditions in particular years. First, we should note that four months before harvest, these matched fields do look to be comparable, as their predictions all cluster around the 1:1 line, meaning that the predicted yields of an irrigated field and its nearest non-irrigated field are close to identical. Surprisingly, this changes dramatically already a month later (LT6), when the vast majority of matches show a much higher predicted yield for the irrigated fields than their non-irrigated neighbours. After LT6, this picture hardly changes, suggesting that irrigation is most important three months before harvest, which approximately corresponds to the booting, heading and flowering stages of winter wheat. Furthermore, different patterns emerge for different years. In 2019, 2021 and 2022, the yield distribution of non-irrigated fields is quite narrow and concentrated around relatively low yields, while the matching irrigated fields vary widely in their yield predictions (but being almost always higher than the non-irrigated fields). In 2018 and 2020, however, the yield predictions of the field pairs are more comparable and for 2018 especially, predicted yields are particularly high for both types of fields. This result is consistent with the findings from Science Case 3 (Figure 13), namely that the total irrigation water amounts for winter wheat were particularly low in 2018. As that year was characterised by heavy rainfall in April and May, crops showed positive yield anomalies regardless of irrigation.

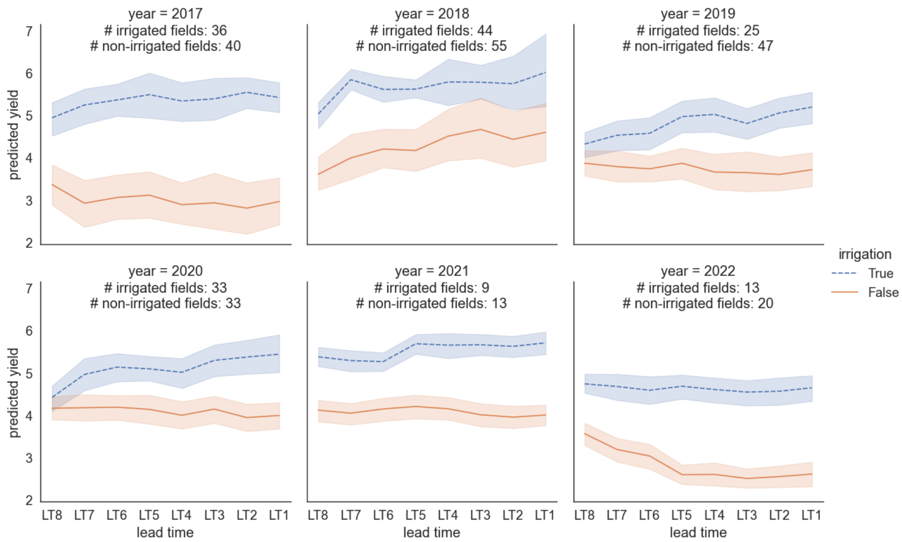

Figure 4: Predicted yield over time for irrigated and non-irrigated fields of common winter wheat for different years. The lines and shaded regions represent the mean and 95% confidence intervals, respectively.

Based on these results, we propose that an irrigation advisory tool could be implemented by tracking how yield predictions based on earth observation of vegetation and soil moisture parameters change over time and/or how they diverge for comparable (e.g. spatially close) fields. As we illustrate for the average field in different years in Figure 4, farmers could be alerted when their fields' yield prediction drops by more than a particular threshold value between two consecutive lead times. They could then be advised to irrigate their fields (more). How much irrigation should be applied could be deducted from extracting the irrigation water amounts of spatially close irrigated fields with the tools developed in Science Case 3. However, we should note that this downscaling approach for irrigation water amounts has not been validated yet and should be subject to a validation study before being used in an advisory tool. Alternatively, a process-based crop model could be employed to find the crop's current irrigation water needs.

Such an approach was envisioned in this demonstration case but was found to be infeasible in its timeframe.

.2.4 Fertilization advisory tool (CG-RS)

Fertilization is one of the key field management practices which farmers can use to improve/stabilize yield quantity and/or quality. Each fertilizer application is the result of three tightly interconnected questions – when, where and how much fertilizer to apply. Nitrogen differs from other nutrients applied: it is the nutrient with the highest impact when applied during vegetation period and the total amount is usually distributed to several applications. The nutrient dosage and its spatial distribution are inferred from two indicators: 1) expected yield and 2) operational dosage adjustment based on plant conditions.

In this demonstration case, we focus on the spatial distribution of the basal nitrogen dosage at the subfield level based on yield spatial variability. In the yield zonation theory, the past information on yield spatial distribution can be used to identify subfield fertilization zones (Blackmore et al., 2003). Recently, the best source of information on yield spatial distribution at the subfield level are the data acquired by the harvest machines. Its main disadvantages are the historical scarcity and missing standardization of its processing (Vega et al., 2019; Arsenoaia et al., 2023). However, the field data can be substituted (to certain extend) by time-series of EO products such as enhanced vegetation index series used by Řezník et al. (2020) and Charvat et al., (2021). Then the potential yield zones of individual fields are typically derived from VI(s) corresponding to selected crop growth stages (CGS) aggregated across several years and normalised by a field's mean/median value. The map of potential yield zones for the whole Czech Republic was calculated by this approach and is available from a map server. The approach how to use such a map to setup fertilizer dose can be divided into two scenarios 1) supporting the high productivity zones or 2) equalizing yield – supporting the low productivity zones.

As the existing map suffers from some sort of temporal instability during certain years, we therefore inspected temporal and spatial correspondence of the EVI index and crop yield data. A different approach to relativize individual field's values of EVI and yields was tested on an extended sub-field level data available within the YIPEEO project.

Data

For this demonstration case we used sub-field level crop yield maps at the Rostenice farm in the Czech Republic. The subfield level data span years 2017 – 2022 and are available only for selected fields due to availability and processing requirements of raw harvester data. The yield data represent crops rapeseed, spring barley, green maize, corn maize, winter wheat, winter barley, but due to lower spatio-temporal coverage of individual crops, only rapeseed, spring barley and corn maize were further analysed (Table 1).

The preprocessing of raw harvester data involves mainly outlier detection, filtration and spatial interpolation as described in Řezník et al. (2020). The resulting sub-field yield maps were produced in 10 m spatial resolution spatially corresponding to grid of the EO data used.

All Sentinel-2 images available for the vegetation seasons of respective years were resampled to 10 m spatial resolution. The EVI index was used as descriptor of vegetation development.

Table 1: Number of fields with sub-field yield data available for Rostenice farm.

	rapeseed	s. barley	Green maize	Corn maize	w. wheat	w. barley
2017	1	2	4	1		
2018	3	5		1		
2019	5	3			1	
2020		5		2	1	1
2021	3	1		5		
2022		2	3	3		3

Methodology

The task which the concept of potential yield zones is aiming for, detection of areas with statistically high/low values of the observed phenomenon, can be also analysed in the GIS using the "hot-spot" analysis. This analysis uses the Getis-Ord GI* statistic - GO (Getis & Ord, 1992) that evaluates observed values by locally calculated Z-score values (EQ).

$$G_i^{*} = \frac{\sum_{j=1}^{n} w_{i,j}x_j - \overline{X}\sum_{j=1}^{n} w_{i,j}}{S\sqrt{\frac{\left[n\sum_{j=1}^{n} w_{i,j}^2 - \left(\sum_{j=1}^{n} w_{i,j}\right)^2\right]}{n-1}}} \qquad (1)$$

where x_j is the attribute value for feature *j*, $w_{i,j}$ is the spatial weight between features *i* and *j*, n is equal to the total number of features and:

$$\overline{X} = \frac{\sum_{j=1}^{n} x_j}{n}$$

$$S = \sqrt{\frac{\sum_{j=1}^{n} x_j^2}{n} - \left(\overline{X}\right)^2}$$

We adopted this method to calculate the GO both for real yield values and for EVI values. Firstly, we analysed the spatial distribution of yield values within a field, as some prior knowledge of it's spatial correlation is required to calculate GO. Individually for each combination of field, year and crop we calculated variogram of yield values and used the it's range value to parametrize the GO calculation. To explore the effect of GO we also calculated mean-normalized value of yield and EVI together with GO. The GO_EVI statistic was than correlated with GO_yield and similarly EVI_norm was correlated with Yield_norm. Then the temporal behaviour of EVI statistics and corresponding correlation was analysed.

Results

The yield variance was calculated in two steps. In the first step the average maximum distance threshold of variance growth was estimated to be 250 m. In the second step effective range of individual variograms was extracted (Figure 1). Then the median value of 194 m which corresponds approximately to 389 neighbouring pixels was used to calculate GO statistic (Figure 2).

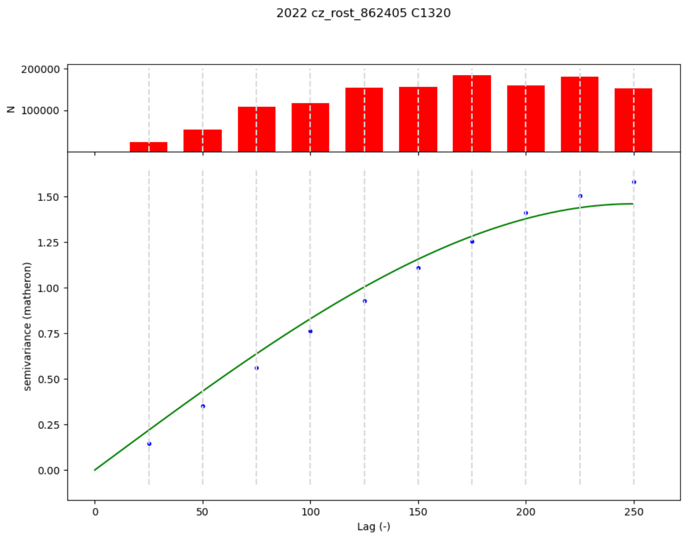

Figure 1: Example variogram of spring barley yield values derived from yield map.

Okomentoval(a): [GU11]: probably numbering has to be changed in respect to the whole document

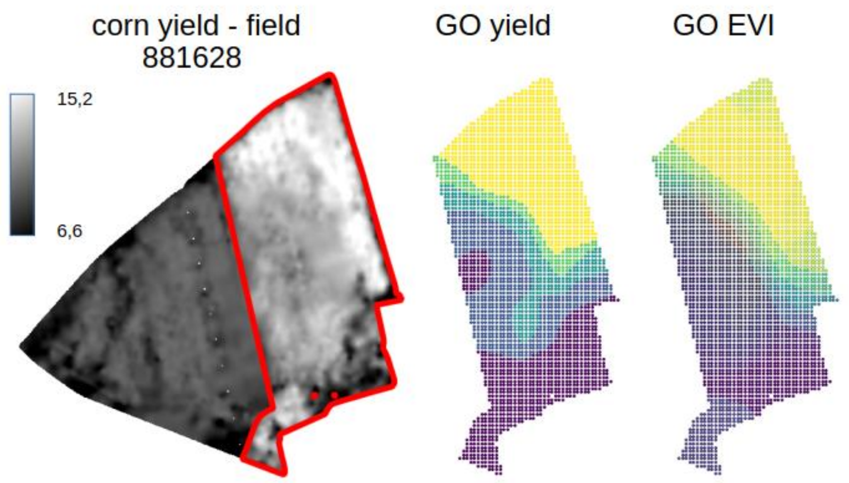

Figure 2: Spatial visualization of Getis-Ord GI statistic (GO) calculated from yield and EVI layers. Gray scale image represents corn maize yield in 2022.*

Both the EVI_norm and GO_EVI show distinct correlation peaks. In case of spring barley (C1320) and rapeseed (I1111) the highest correlation can be usually observed between very end of May and 2/3 of June, whereas in case of corn maize (C1500) the high correlation values are more often between second 2/3 of August and first week of September (Figures 3 - 6).

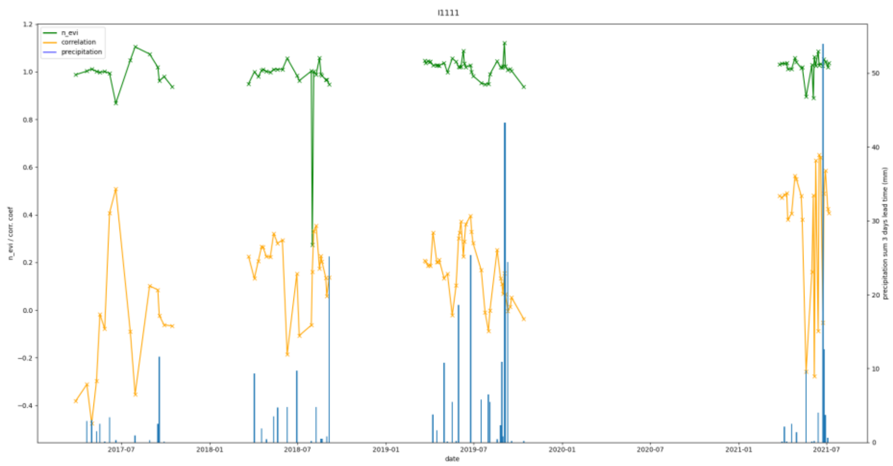

Figure 3: Timeseries of mean-normalized EVI index (EVI_norm) and it' s Pearson correlation coefficient with mean-normalized yield values (rapeseed). EVI_norm is represented by median values on individual S2 acquisition dates.

Figure 4: Timeseries of EVI Getis-Ord GI statistic (GO_EVI) and it' s Pearson correlation coefficient with yield GO values (rapeseed). GO_EVO is represented by median values on individual S2 acquisition dates.*

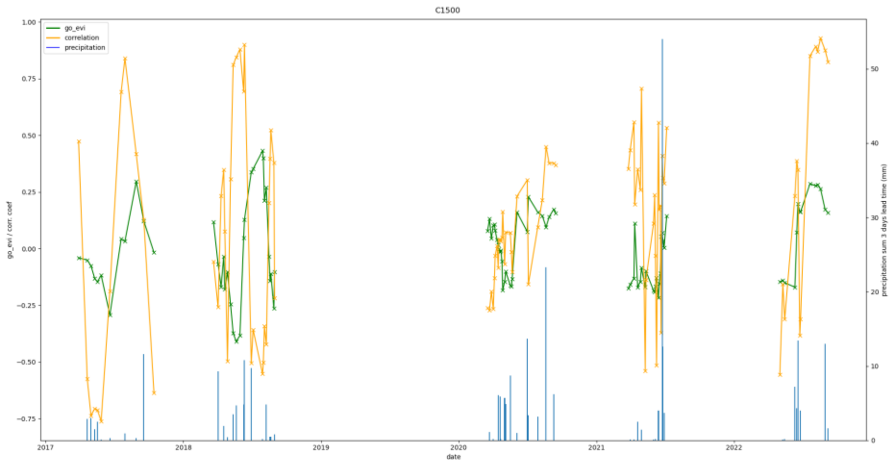

Figure 5: Timeseries of EVI Getis-Ord GI statistic (GO_EVI) and it' s Pearson correlation coefficient with yield GO values (corn maize). GO_EVO is represented by median values on individual S2 acquisition dates.*

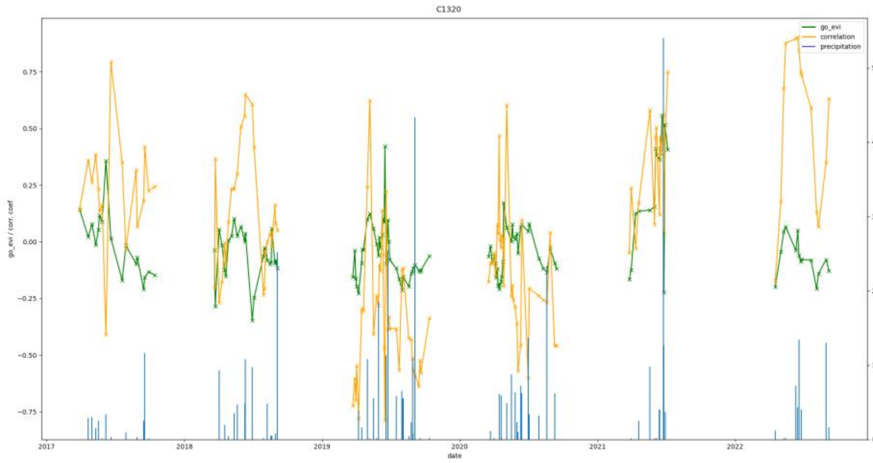

Figure 6: Timeseries of EVI Getis-Ord GI statistic (GO_EVI) and it' s Pearson correlation coefficient with yield GO values (spring barley). GO_EVO is represented by median values on individual S2 acquisition dates.*

Discussion

Both EVI statistics showed similar pattern of close correlation with corresponding yield statistics. The closer correlation in June for spring barley and rapeseed and in August for corn maize broadly corresponds with other studies reporting close correlation according to CGS (BBCH 40-50). The GO_EVI statistic usually reached closer correlation peaks than the EVI_norm version. That is suggesting that the more spatially constrained normalization technique could lead to more precise prediction of relative yield distribution within individual fields. This difference might be related to substantially stronger transformation of the mutual relationship in case of GO statistic. The scatter plots of GO statistics could indicate some clustering, which might be interesting to analyse with respect to its localization in real space and potentially with respect to environmental variables. Second and more urgent question is the method of temporal aggregation together with data source used. The previous studies usually aggregated the data by calculating average/median value of EVI index across years and crops but respecting the CGS. The effect of methods similar to those used for composing cloud-free mosaics could be evaluated.

References

Arsenoaia VN, Ratu R, Velescu I, Tenu I. Field tests of a John Deere harvester for the purpose of production maps achievement. Lucrări Ştiinţifice. 2023; 66(1)

Blackmore, S., Godwin, R. J., & Fountas, S. The analysis of spatial and temporal trends in yield map data over six years. Biosystem Engineering. 2003; 84(4), 455-466

Getis A, Ord JK. The Analysis of Spatial Association by Use of Distance Statistics. Geographical Analusis. 1992; 24(3)

Charvát, K., Lukas, V., Charvát, K., Horáková, Š. Delineation of Management Zones Using Satellite Imageries. In: Södergård, C., Mildorf, T., Habyarimana, E., Berre, A.J., Fernandes, J.A., Zinke-Wehlmann, C. (eds) Big Data in Bioeconomy. 2021; Springer, Cham. https://doi.org/10.1007/978-3-030-71069-9_18

Řezník T, Pavelka T, Herman L, Lukas V, Širůček P, Leitgeb Š, Leitner F. Prediction of Yield Productivity Zones from Landsat 8 and Sentinel-2A/B and Their Evaluation Using Farm Machinery Measurements. Remote Sensing. 2020; 12(12):1917. https://doi.org/10.3390/rs12121917

Vega, A., Córdoba, M., Castro-Franco, M., Balzarini, M. Protocol for automating error removal from yield maps. Precision Agriculture. 2019; 20, 1030-1044